The DOI for this manuscript is doi: 10.1175/JAMC-D-16-0304.1

The final published version of this manuscript will replace the preliminary version at the above DOI once it is available.

If you would like to cite this EOR in a separate work, please use the following full citation:

Thurai, M., P. Gatlin, V. Bringi, W. Petersen, P. Kennedy, B. Notaros, and L. Carey, 2016: Towards Completing the Rain Drop Size Spectrum: Case Studies Involving 2D-Video Disdrometer, Droplet Spectrometer, and Polarimetric Radar Measurements. J. Appl. Meteor. Climatol. doi:10.1175/JAMC-D-16-0304.1, in press.

# Towards Completing the Rain Drop Size Spectrum: Case Studies Involving 2D-Video Disdrometer, Droplet Spectrometer, and Polarimetric Radar Measurements

Merhala Thurai[1], Patrick Gatlin[2], V. N. Bringi[1], Walter Petersen[2], Patrick Kennedy[3], Branislav Notaros[1] and Lawrence Carey[4]

[1]Department of Electrical and Computer Engineering, Colorado State University, Fort Collins, CO

[2]NASA-MSFC Earth Science Office, National Space Science and Technology Center, Huntsville, AL

[3]CSU-CHILL Radar facility, Colorado State University, Greeley, CO

[4]University of Alabama, Huntsville, AL

Revised manuscript submitted to:

Journal of Applied Meteorology and Climatology

December 2016



---

*Corresponding author address:* M. Thurai, Department of Electrical and Computer Engineering, Colorado State University, Fort Collins, Colorado, 80523
E mail: merhala@engr.colostate.edu

# ABSTRACT

Analysis of drop size distributions (DSD) measured by collocated Meteorological Particle Spectrometer (MPS) and a 3rd generation, low-profile, 2D-video disdrometer (2DVD) are presented. Two events from two different regions (Greeley, Colorado, and Huntsville, Alabama) are analyzed. Whilst the MPS, with its 50 μm resolution, enabled measurements of small drops, typically for drop diameters below about 1.1 mm, the 2DVD provided accurate measurements for drop diameters above 0.7 mm. Drop concentrations in the 0.7 to 1.1 mm overlap region were found to be in excellent agreement between the two instruments. Examination of the combined spectra clearly reveals a drizzle mode and a precipitation mode. The combined spectra were analyzed in terms of the DSD parameters, namely the normalized intercept parameter, $N_W$, the mass weighted mean diameter, $D_m$, and the standard deviation of mass spectrum, $\sigma_M$. The inclusion of small drops significantly affected the $N_W$ and the ratio $\sigma_M/D_m$ towards higher values relative to using the 2DVD-based spectra alone. For each of the two events, polarimetric radar data were used to characterize the variation of radar measured reflectivity ($Z_h$) and differential reflectivity ($Z_{dr}$) with $D_m$ from the combined spectra. In the Greeley event, this variation at S-band was well-captured for small values of $D_m$ (< 0.5 mm) where measured $Z_{dr}$ tended to 0 dB but $Z_h$ showed a noticeable decrease with decreasing $D_m$. For the Huntsville event, an overpass of the Global Precipitation Measurement mission Core satellite enabled comparison of satellite-based dual-frequency radar retrievals of $D_m$ with ground based DSD measurements. Small differences were found between the satellite-based radar retrievals and disdrometers.

## 1. Introduction

Knowledge of the drop size distribution (DSD) at different scales and in different rainfall types and rain intensities is of obvious importance in both practical radar applications as well as in numerical parameterizations of the fundamental microphysical processes such as collision-coalescence, drop break-up and evaporation. Due to the large variability of the DSD (Bringi et al., 2003, Ulbrich 1983), it has been conventional (depending on application) to consider moments of the DSD such as mass-weighted mean diameter ($D_m$), normalized intercept parameter ($N_W$) and width of the mass spectrum ($\sigma_M$) as well as the shape of the normalized and scaled distribution (e.g., Ulbrich and Atlas 1998; Testud et al 2001; Haddad et al. 1996; Semper-Torres et al, 1994; Lee et al. 2004). Whilst the higher order moments (>=3) involved in calculating $D_m$, $N_w$ or $\sigma_M$ are generally considered to be much less sensitive to the small and tiny drop end of the DSD (typically diameters < 0.7 mm), both the total number concentration (zeroth moment) and the shape of the distribution can be significantly controlled by the small drop end which is difficult to measure accurately.

The DSD is generally measured at the surface using optical or impact-type disdrometers typically averaged over several minutes to capture the distribution of the aforementioned DSD parameters with rain rate. It is also well-known that most, if not all, disdrometers tend to underestimate the concentration of small and tiny drops (D < 0.7 mm or so) because of sensitivity issues and poor resolution, and – depending on the design – other instrumental factors may also play a role (Tokay et al. 2001; Miriovsky et al. 2004). The accurate measurement of tiny drops is important for the calculation of the total concentration of drops ($N_{tot}$), as well as in the numerical modeling of collision-coalescence processes of rain formation and DSD evolution (e.g., Meyers et al. 1997; Milbrandt and Yao 2005). For example, the probability that a large drop will undergo collisions with a tiny drop is proportional to (among other factors) the concentrations of the latter. Ideally, such concentrations should be measured with very high resolution instruments developed for airborne applications (e.g., 2D-C or cloud imaging probe) but these have been rarely used as surface disdrometers (Montero-Martinez et al. 2009).

More importantly for polarimetric radar applications, collisions between moderate-to-large drops ($D > 2$ mm or so) with tiny drops ($D \sim 0.5$ mm) has long been postulated as a viable mechanism of producing large amplitude oscillations in the larger drop (possible precursor to drop break-up) that can be sustained against viscous dissipation (Beard et al. 1983). The excess kinetic energy due to collisions (or simply collision kinetic energy) which can force such oscillations is proportional to (among other factors) the volume of the tiny drops, so their sizes should also be measured with high resolution. Johnson and Beard (1984) determined that the most energetic collisions were those between moderate-to-large drops ($D > 2$ mm) and tiny drops in the range ($D \sim 0.3$–$0.8$ mm). This re-emphasizes the importance of measuring the tiny drops with higher resolution than is possible with current surface disdrometers.

The gamma DSD model (Ulbrich, 1983)is widely used in polarimetric and dual-wavelength radar applications but the shape parameter ($\mu$, as defined in Ulbrich and Atlas, 1998).) and its dependence on rain microphysics is not well-established via surface distrometer measurements principally due to difficulty in measuring the concentrations at the small drop end which plays a strong role in estimating the $\mu$-parameter. Assumptions of constant $\mu$ ($\approx 3$), or empirical $\mu$–$\Lambda$

(where $\Lambda D_m=4+\mu$) fits, or statistical methods based on fits to $\sigma_M$-$D_m$ variations are susceptible to errors which are not easily quantified (e.g., Kozu et al., 2009; Zhang et al.2003; Williams et al, 2014). On the other hand Testud et al. (2001) found remarkable stability of shape of the normalized and scaled DSD (non-gamma model) using aircraft-based imaging probes in oceanic rainfall. It is not clear if a single gamma model can be used to describe the shape of the entire DSD (e.g., Able and Boutle 2012). While there is vast literature on DSD measurements based on surface disdrometers or aircraft imaging probes, very few studies accurately characterize the full size spectrum which needs at least 2 instruments and an overlapping size range to ensure that instrumental errors are low (i.e., to ensure consistency and continuity of concentration measurements in the overlap size range), and that the resulting data can be used for physical interpretation of the DSD shape and variability.

In this paper we describe DSD data collected with 'side-by-side' collocation of the Meteorological Particle Spectrometer (MPS; Baumgardner et al. 2002) with a 3rd generation, low-profile, 2D-video disdrometer (2DVD; Schönhuber, et al., 2008) to enable us to characterize the concentration of the tiny drops with very high resolution (50 μm) with the MPS, and the same for larger drops (with resolution of 170 μm) from the 2DVD. Our objective then is to combine the MPS and 2DVD data to form a composite DSD with high resolution at the small drop end provided by the MPS and good resolution provided by the 2DVD for moderate-to-large drops. So far, measurements at two locations have been carried out, namely Greeley, Colorado, and Huntsville, Alabama, and we report here on observations and analysis from two long duration events from the two sites.

## 2. Instrumentation and experimental set-up

### *a. The Two Campaigns*

The Greeley campaign took place from April to October 2015 and the Huntsville campaign started in March 2016. The same MPS and the 2DVD instruments were used in the Greeley campaign and the Huntsville campaign.

At the Greeley site, both instruments were conveniently installed within a 2/3-scaled double fence inter comparison reference (small DFIR, the standard adopted by the National Weather Service for snow gages) windshield, located at about 13 km SSE from the CSU-CHILL S and X-band polarimetric radar site (Bringi et al., 2011). The sensor areas of the disdrometers were set at a height which is 13 inches below the top of the inner fence. The small DFIR had been originally built for a snow observation campaign and had proven to be effective in substantially reducing wind speeds (Fig. 17 in Notaros et al., 2016). A Pluvio weighing bucket-type rain gauge was also installed within the wind fence. This was a 2$^{nd}$ generation weighing type rain gauge manufactured by OTT with a 200 cm$^2$ collection area that utilizes a highly precise load-cell to enable study of rainfall amounts as little as 0.1 mm with an accuracy of 0.2% (OTT Messtechinik GmbH 2010).

In Huntsville, Alabama a similar small DFIR located at the National Space Science and Technology Center (NSSTC) on the campus of the University of Alabama in Huntsville (UAH) housed the MPS and the 2DVD. The sensor areas were also set at the same height as in the

Greeley campaign. The site is located 15 km from the UAH/WHNT-TV Advanced Radar for Meteorological and Operational Research; (ARMOR), which is a C-band polarimetric radar (Petersen et al. 2005, http://www.nsstc.uah.edu/armor/). Fig. 1(b) shows the ground instruments and the small DFIR configuration at the Huntsville site.

*b. Small Drop Measurements with MPS and Overlap with 2DVD*

The MPS uses a linear array of 64 photodiodes to measure the shadow images of particles falling through a collimated laser beam. The concepts of the technique were originally introduced by Knollenberg (1970), and later by Baumgardner et al. (2002). This instrument has 50 micron resolution and is suitable for measuring small drops. The size range is 50 microns to 3.1 mm and its sampling area is 6.2 $cm^2$. The 2DVD on the other hand has a much larger 10 by 10 $cm^2$ sensor area (Schönhuber, et al., 2008) but the pixel resolution for the front and side view (silhouettes) is around 170 microns.

The 2DVD is a well-established disdrometer that uses two optical cameras to measure the size, shape and fall velocity of individual raindrops (Schönhuber, et al., 2008). Of all the disdrometers, this instrument has been established as the most suitable instrument for measuring the large drop end of the DSD spectrum (Gatlin et al., 2015). On the other hand, this instrument does not reliably measure the drop concentration for drop diameters less than about 0.6 mm; in fact, it tends to underestimate N(D) for these small drops (Tokay et al., 2001). The problem is related to lowered sensitivity to small and tiny drops, the associated difficulty in matching of these drops from the two camera images and to finite instrument resolution.

The MPS is a high resolution instrument for drop imaging and measurement of the DSD specifically designed for fixed site operation (see Fig. 2 and Table 1). It was developed in early 2000 to measure drizzle for the National Weather Service. Fall speeds are measured with the MPS after sizing the horizontal dimension (or the width '*a*' in Fig. 2b) and dividing by the time taken to traverse the photo-detector array (spherical shape is assumed, i.e., vertical dimension is equal to '*a*'). Table 1 gives some of the important technical specifications of the MPS and the 2DVD.

The fall speed accuracy of the MPS depends primarily on the digitization error (±25 μm), and according to the manufacturer it is 10% for $D = 0.25$ mm and 1% for $D = 1$ mm. The factors that determine the accuracy of the 2DVD for size, fall speed, and axis ratio are given in Schönhuber et al. (2008), Kruger and Krajewski (2002), and Thurai and Bringi (2005).

The effective measurement area of the MPS decreases with increasing drop width ("entire in" images; Heymsfield and Parrish 1978) and is a factor of ≈ 30 smaller relative to the 2DVD for a measured drop width of 1.5 mm. This increases the sampling error for estimation of the concentration of drops with $D \approx 1.5$ mm by a factor of $\sqrt{30} \approx 5.5$. In our application, we will utilize the MPS for measurement of small drops with $D < 1.2$ mm and to compare the measurements with the 2DVD in the overlap region of $D \approx 0.7$–$1.2$ mm to ensure consistency of observations. The method of deriving the drop size distribution from the MPS is summarized in the Appendix.

## 3. The Greeley Campaign

The event considered in this paper occurred on 17 April 2015, soon after the MPS installation at the small DFIR site at Greeley. This event was part of a mid-latitude synoptic scale cyclone that had produced fine drizzle, light precipitation, cold rain, rain bands (both stratiform and convective in nature) as well as thunderstorms towards the end of the event (Thurai et al., 2015). The CSU-CHILL S-band radar scans were made at regular and closely spaced time intervals and consisted of surveillance plan position indicator (PPI), sector PPI, and range-height indicator (RHI) scans. The preprogrammed scan sequence included (a) a 360 scan at 10 deg elevation, (b) two-sweep RHI scans over the disdrometer site, and (c) a one sweep (1.5 deg elevation) PPI sector volume centered over the disdrometer site, which were repeated every 5 min and 27 seconds.

### *(a) Ground instrument data*

(I) Fall velocities

The 17 April 2015 event (Greeley Event) was an intermittent but long duration event which produced a variety of rain types over a period of 20 hours. Whilst the MPS enabled drop concentration measurements down to 0.1 mm (i.e. with at least 2 pixels), the 2DVD recorded drops as large as 5 mm associated with the (non-hail producing) thunderstorm. Fall velocities showed a clear trend with drop diameter, in agreement with the expected Gunn-Kinzer variation, but with an adjustment factor appropriate for the 1.4 km altitude for Greeley. Fig. 3(a) shows the comparisons for all drops. Fig. 3(b) shows the distribution of velocity for drops with equivalent spherical diameters ($D_{eq}$or D) of 2.5 ± 0.1 mm. The increased fall velocities can be clearly attributed to the reduced pressure at the 1.4 km height above mean sea level (AMSL).

(II) Rain rates and accumulations

The processed Pluvio data are shown in Fig. 4: (a) shows the 1-minute rain fall rate, (b) shows the rainfall accumulation, and (c) shows the corresponding 2-hour total accumulation. The 1-minute rain rate was as high as 19 mm/h (towards the end of the event), the total event accumulation over the 20 hour duration was 17 mm, and the 2-hour accumulations varied significantly throughout the event, ranging from 0.05 mm to 4.91 mm.

Based on the rainfall rates and other ground instrumentation data as well as the corresponding CHILL scans for the entire event duration, a broad rain-type classification for each of the 2-hour period (corresponding to Fig. 4(c)) was made, as given in Table 2. Note the highest rainfall rate occurred during the thunderstorm period (18 - 20 UTC), and the lowest rain accumulation occurred during the fine drizzle period (10 – 12 UTC). (Here we have adopted the AMS glossary description of drizzle as ‘form of precipitation consisting of water droplets less than 0.5 mm in diameter and larger than 100 nm.)

(III) Drop size distributions

For drop size distribution comparisons between the 2DVD-based and the MPS-based measurements, we first split the entire time series event into the same 2-hour time intervals mentioned earlier, starting with 02:00 UTC and ending with 20:00 UTC. Fig. 5 shows these 2-

hour DSD comparisons, except for the last two hours. The diamonds represent the MPS-based DSD's and the crosses represent the 2DVD-based DSD's. Close overlap is seen in the 0.7 - 1.2 mm drop diameter range. For over 95% of the cases, the fractional differences between the MPS and the 2DVD drop concentrations (on a log scale) in this diameter range was less than 10%, and moreover the overall average was found to be -3.8% which is very close to zero, indicating that there is no systematic bias. The log-log scale was used to focus on the small drop size range. The concentration of smaller drops was underestimated by the 2DVD relative to the MPS, as expected. However, the 2DVD measurements of moderate to large drop sizes (drop volume is based on two orthogonal views) can be considered to be more accurate than the MPS, since the latter assumes *apriori* spherical drop shapes.

As a result of the consistency between the two instruments demonstrated in Fig. 5, the full DSD spectra were constructed based on the drop concentrations from the MPS for $D_{eq} < 0.7$ mm and the 2DVD-based drop concentrations for $D_{eq} \geq 0.7$ mm. Examination of Fig. 5 reveals two different modes, (i) a drizzle component for $D_{eq} \leq 0.5$ mm and (ii) a precipitation mode for larger diameters (starting near or about the shoulder region especially noticeable in the 04:00-06:00 UTC panel). Such modes have been previously identified from aircraft imaging probe (2D-Cloud and 2D-Precipitation) data collected in warm rain clouds analyzed by Able and Boutle (2012). In fact, their combined spectra from the 2D-C (similar to MPS) and 2D-P (similar to 2DVD) are very similar in shape to Fig. 5. They also show that an exponential shape forms a good fit to the precipitation mode portion of the combined spectra (easy to see as a straight line in a more conventional semi-log plot of the DSD). Our MPS-2DVD results are consistent with their analysis in spite of different instruments, time integration and meteorological conditions (in-cloud oceanic warm rain versus continental spring-time surface precipitation).

Fig. 6 shows the comparisons of two DSD parameters based on the 1-minute DSDs from the combined spectra (shown as black dashed line) and those solely from 2DVD (grey crosses). The two parameters are the mass-weighted mean diameter ($D_m$) shown in panel (a) and the standard deviation of the mass spectrum ($\sigma_M$) shown in panel (b), as defined in Ulbrich and Atlas, (1998). During the thunderstorm period (18:00 – 20:00 UTC) rapid fluctuations can be seen in both parameters, and this correlates well with the rapid fluctuations in rain rates from Pluvio measurements shown earlier in Fig. 4(a).

The inclusion of the small drops from the MPS in the combined spectra results in a decrease in $D_m$ and an increase in $\sigma_M$. The resulting variation of $\sigma_M$ versus $D_m$ for the combined spectra (diamonds) is shown in panel (c) and compared with those based on 2DVD data alone (crosses). The dashed line in panel (c) represents the best-fitted power law equation - using log-linear model - for the variation based on the 2DVD data alone. Note the power-law fitted equation is close to that given in Thurai et al. (2014) and Williams et al. (2014) who used 2DVD data alone from a long measurement campaign in Huntsville, AL. For the combined DSDs, it was not possible to fit a representative power-law equation (of the form $\sigma_M = \alpha D_m^{\beta}$) for the entire dataset primarily because the $\sigma_M$ estimates become noisy for low $D_m$, e.g., between 10 – 12 UTC in panels (a) and (b). If the fit is performed for the data with $D_m \geq 0.5$ mm, the fitted equation becomes $\sigma_M = 0.48\ D_m^{0.94}$ for the combined spectra which is significantly different from the fitted equation using the 2DVD spectra alone ($\alpha$=0.29, $\beta$=1.44).

Fig. 7 shows a set of $D_m$ histograms based on the 2DVD-based DSDs and the combined DSDs. The three top panels correspond to the 2-hourly periods of 02:00–04:00, 08:00–10:00 and 18:00–20:00 UTC, corresponding to convective rain, light rain or stratiform rain, and thunderstorm. The following summarizes some pertinent points:

i. Histograms from the combined spectra show lower values of $D_m$ than those from the 2DVD alone.
ii. Light stratiform rain produces histograms with lower $D_m$ than convective rain (as expected).
iii. There is considerable difference between the modal values of $D_m$ in light rain (mostly non-overlapping histograms)
iv. The thunderstorm period histograms are similar for larger $D_m$ but the MPS-2DVD based DSDs have more cases with low $D_m$ ($\leq$ 0.5 mm).

The lower panels in Fig. 7 show the $D_m$ histograms classified in terms of four rain rate intervals. The very low rain rates with R < 0.5 mm/h (including drizzle) shows skewed histograms for both cases, but the combined DSDs give rise to noticeably lower $D_m$ values. The histogram shows a peak of around 0.15 mm for the combined DSDs versus 0.6 mm for the 2DVD-based DSD's. The histograms become more similar for the higher rain rates, exhibiting peaks at around 1 mm for the 1<R<5 mm/h interval. For R > 5 mm/h, the peaks are around 1.15 mm, but the total number of points was only 27.

Fig. 8(a) compares the $D_m$ calculated using only the 2DVD spectra versus those using the combined spectra. Compared with the [1:1] dashed line, the bias is evident, and in almost all cases, the 2DVD-only spectra tend to overestimate $D_m$, which is to be expected, but the overestimation is higher when $D_m < 1$ mm (i.e., for DSDs where small drops play a more dominant role). Note, also, that the $D_m$ calculated from the 2DVD-only spectra shows a floor at 0.5 mm since the small drop concentrations are strongly underestimated.

In terms of rain accumulation, the addition of the small drops from the MPS provided small but significant improvement in the agreement with the collocated Pluvio data for the two convective rain event periods (02-04 UTC, and 04-06 UTC). Table 3 shows the comparisons for the 2-hour period. Also shown are the comparisons for the 18-20 UTC time period which included modest thunderstorm activity. In all three cases, the 2-hour accumulations from the composite MPS-2DVD DSDs show better agreement with Pluvio data. For other two hour periods, accumulations were less than 2 mm.

### *b) S-band CHILL Radar observations*

As mentioned earlier, the CHILL S-band radar scans were made over the instrumented site at regular and closely spaced time intervals (< few minutes). From the surveillance and sector PPI scans, values of $Z_h$ and $Z_{dr}$ over the instrument site were extracted (az: 171.5 deg, range 13 km). Only the radar pixel directly above the instrument site was considered, and no spatial averaging was done. The radar pulse volume was centered at ~310 m above the disdrometer site (which was around 30 m higher than the radar site). Fig. 9 (a) and (b) shows the variation of these values versus $D_m$ derived from the 1-minute DSDs (but smoothed over 3-minutes) with the S-band $Z_h$

and $Z_{dr}$ extracted over the instrument site. The grey crosses represent the $D_m$ values obtained from the 2DVD spectra alone and the black diamonds represent those derived from the 2DVD-MPS combined spectra.

Some important points can be noted from Fig. 9(a) and (b). First, the $Z_{dr}$ - $D_m$ variation does indeed get affected by including MPS measurements of small drops, particularly for low $D_m$ values. Second, when $D_m$ goes below 0.5 mm, the S-band $Z_{dr}$ becomes very close to 0 dB and exhibits very little sensitivity to further lowering of $D_m$ (to be expected as the small drops are close to spherical in shape). On the other hand, $Z_h$ exhibits greater sensitivity to changes in $D_m$ even below 0.5 mm for the combined DSDs. Thus, for events with low $D_m$ (<0.5 mm) the combined spectra/CHILL radar data suggests the appropriateness of using both $Z_h$ and $Z_{dr}$ to retrieve $D_m$ (as opposed to using $Z_{dr}$ alone), see Thurai et al. (2012).

# 4. The Huntsville Campaign

*a) Event description*

Huntsville has a very different climate to Greeley, and its altitude is 200 m AMSL compared with 1.4 km AMSL for Greeley. The climate of northeastern Colorado is much drier and cooler on average than that of northern Alabama. Huntsville receives an average of 138 cm of precipitation each year whereas Greely receives less than 38 cm each year. Greely has a daily mean temperature that is 4 degrees cooler than Huntsville. According to the Köppen-Trewartha climate classification system (Trewartha and Horn 1980), this labels Greeley, CO as a semi-arid type climate, whereas Huntsville, AL is a humid subtropical type climate (Belda et al. 2014).

The Huntsville event considered in this paper occurred on 11 April 2016, and consisted of precipitation associated with the mesoscale vortex of a developing squall line that moved across northern Alabama between 1700 to 2300 UTC and produced over 25 mm of rainfall in the Huntsville area. This event was sampled by the MPS and 2DVD just after they had been installed within the small DFIR. The ARMOR radar was performing PPI scans over these disdrometers, and the Global Precipitation Measurement (GPM) mission Core satellite (Hou et al. 2014) made an overpass of northern Alabama near the end of this precipitation event.

*b) Ground-based measurements*

Fall velocity measurements from the 11 April 2016 event are shown in Fig. 10(a). Once again the dashed line represents the Atlas et al. (1973) fitted equation to the G-K data at sea level. The 2DVD measurements show much closer agreement to this variation than the Greeley data shown earlier in Fig. 1(a). However, note the more intense color contours lie slightly higher than the dashed line, which can be explained by the 200 m altitude above sea level. Fig. 10(b) shows the histograms of vertical velocity specific for all drops with $D_{eq}$ values of $2.5 \pm 0.1$ mm, whose mode closely agrees with the expected fall velocity of 7.3 m $s^{-1}$.

For drop size distribution comparisons between the 2DVD-based and the MPS-based measurements, the time series event was split into 1-hour time intervals, starting at 17:00 UTC and ending at 23:00 UTC. Fig. 11 shows these hourly DSD comparisons. The black diamonds represent the MPS-based DSDs and the black crosses represent the 2DVD-based DSD's. Fig. 11 shows similar features to Fig. 5, that is, close overlap in the 0.7 - 1.2 mm drop diameter range between the MPS-based DSDs and the 2DVD-based DSDs, but again for smaller drops, the 2DVD underestimates the drop concentration compared with the MPS.

As with the Greeley data analysis, the combined spectra were constructed based on the drop concentrations from the MPS for $D_{eq} < 0.7$ mm and the 2DVD-based drop concentrations for $D_{eq} \geq 0.7$ mm. As discussed in Section 3.1(c), the two modes identified by Able and Boutle (2012) are quite evident in Fig. 11—a drizzle mode for diameters < 0.5 mm, and a precipitation mode starting around 0.7-1 mm (i.e., the shoulder region) and extending to the largest sizes. These two modes are actually more prominent in Fig. 11 as opposed to Fig. 5 perhaps due to the expected prevalence of warm rain processes in the Huntsville event, which had a 0°C level around 3 km AGL, as opposed to dominance of ice phase processes in the Greeley event, which had a 0°C level much lower (for example at 05:44 UTC, the LDR from a 10 degree VAD scans had shown extraordinarily clear melting layer around 6 km range as in Fig. 3 in Thurai et al., 2015) which gives a melting layer height of around 1 km AGL).

Fig. 12 (a) and (b) show, respectively, the time series comparisons of $D_m$ and $\sigma_M$ derived from the 1-minute DSDs from the combined data from MPS and 2DVD (shown as black diamonds) and those from 2DVD data alone (grey crosses), over a period of 4 hours. The same trend as the Greeley results is seen, that is, the MPS-2DVD combined spectra give rise to slightly lower $D_m$ and larger $\sigma_M$ relative to using the 2DVD spectra alone. Panel (c) of Fig. 12 shows the corresponding effect on $N_W$. The higher concentration of small drops in the combined spectra results in an increase in $N_W$. Note that the definition of the normalized intercept parameter follows Testud et al. (2001) (which is independent of the gamma assumption) and, except for constant terms, is proportional to the ratio of rain water content to $D_m^4$. The increase in the total number concentration will be even more significant (not shown here).

### *c) ARMOR radar data*

The radar used for the Huntsville campaign is the C-band ARMOR radar, located 15 km from the ground instrumentation site. The ARMOR scanning strategy for the 11 April 2016 event consisted of plan position indicator (PPI) type (i.e., radar antenna rotates 360 degrees in azimuth) scans with a repeat cycle of every 2.5 minutes. From these scans, the radar data over (and surrounding) the disdrometer site were extracted (52 deg azimuth, 15 km range, and once again only the radar pixel directly above the instrument site was considered, and no spatial averaging was done.). The chosen elevation angle was 1.3 deg. Given that the half-power antenna beamwidth is close to 1°, the cross-beam resolution will be around 250 m at the range of 15 km. The height of the radar pixel above ground will be around 340 m.

The $Z_h$ and $Z_{dr}$ data extracted from the ARMOR PPI scans over the disdrometers are shown in Fig. 13 (a) and (b), respectively, as a time series for the same 20:00 – 24:00 UTC time period. In panel (b), the $D_m$ values obtained from the combined DSDs are also included (the same as the diamonds in Fig. 12a). One can see good correlation between the ARMOR $Z_{dr}$ values and the combined disdrometers-based $D_m$ values.

The correlation between $Z_{dr}$ and $D_m$ is better depicted in Fig. 13c as a scatter plot which shows ARMOR $Z_{dr}$ versus the ground based $D_m$ data from 2DVD spectra as well as the combined spectra. The C-band $Z_{dr}$ is more sensitive to $D_m$ change than at S-band. However, the $D_m$ values for the Huntsville event did not go below 1 mm, and as noted in Thurai et al. (2012), $Z_{dr}$ alone is sufficient to estimate $D_m$ for such cases. Note that for a given radar measured $Z_{dr}$, the $D_m$ from the combined spectra is typically biased low relative to the $D_m$ from the 2DVD spectra (around a few tenths of a mm at $Z_{dr}$ of 1.5 dB). This trend is noted even in the presence of radar measurement errors inherent in the scatter in panel (c).

### *d) GPM overpass*

An overpass of the GPM Core satellite during this Huntsville event enabled us to examine the performance of Version 4 of the DPR Level 2 algorithm (2ADPR), which assumes a fixed $\mu = 3$ in order to retrieve Dm and Nw from the attenuation corrected reflectivity values computed at the two frequencies (Iguchi et al. 2016). The $D_m$ value from the DPR bin closest to the disdrometer site was 1.9 mm, and the average from this bin and the surrounding bins was 1.8 mm with a standard deviation of 0.1 mm (Figure 14a). These values were derived from DPR measurements at 23:31:44 UTC. Over a five minute period around this time, the average $D_m$ values from the 2DVD and combined MPS-2DVD was 1.73 mm and 1.61 mm, respectively (Fig 12a). The average Nw computed by the 2ADPR Version 4 algorithm was lower than that measured by the disdrometers. The nine bin average Nw from the DPR (Fig. 14b) was 828 m-3mm-1 (2.92 in log10 units) with a standard deviation of 189 m-3mm-1, whereas for the 2DVD and combined MPS-2DVD the average Nw over the five minute period was 1348 ($\log_{10}$=3.13) and 1952 $m^{-3}mm^{-1}$ ($log_{10}$=3.29), respectively. The $\sigma_M$ measured from the MPS-2DVD over this five minute period was 0.76 mm, which for a gamma DSD yields a μ value of 0.49.

Finally, in Fig. 14(c) we show the 10 minute DSD measurements from the MPS and 2DVD during the GPM overpass time in order to illustrate the DSD agreement in the overlap region for a finer time resolution (rather than over a 1 hour or two hour period). Although the MPS data are somewhat more noisy, thee two DSDs once again merge rather well in the 0.7 – 1.2 mm diameter region.

## 5. Discussion

### *(a) DSD shape*

In the past, DSD measurements at a given site have been carried out largely with the same type of instrument, most of which can measure across a similar range of diameters (e.g. Parsivel disdrometer,Joss-Waldvogel disdrometer and/or 2DVD, etc.). Krajewski et al. (2006) have compared DSD measurements from different instruments which were located close to one another and found considerable instrument-to-instrument differences which made it difficult to study the natural variations in DSD at short spatial scales (< few hundred meters). Results reported herein from two rain events in different climatologies show that there is very close agreement between the 2DVD and the MPS spectra in the overlap region (0.7–1.5 mm drop diameter) giving confidence that the combined spectra can be used to characterize the entire DSD more accurately than hitherto possible with single instruments. The fact that both instruments were installed within identical DFIR wind shields may have been responsible in that the wind-induced effects could have been significantly reduced, especially for the MPS. On average the mean wind speed inside the DFIR was reduced by a factor of three or more relative to the environment outside the fence at the Greeley site (for example, Fig. 17 in Notaros et al. 2016). This allowed us to operate the MPS without its wind vane inside the small DFIR so the laser beam was oriented parallel to the expected environmental mean wind direction at both sites to help mitigate size distortion that can arise due to the horizontal motion of the drops.

The combined MPS-2DVD spectra from both the Greeley and the Huntsville sites have clearly shown that (in the events analyzed herein and over 1-2 h time integration), the concentration of small drops does increase significantly with decreasing drop diameter (D <~ 0.5 mm) and is consistent with the drizzle mode identified by Able and Boutle (2012). Our combined MPS-2DVD spectral shapes are also consistent with what they identified as the precipitation mode for sizes > 0.7 mm which in the log-log plots of N(D) versus D, starts with a well-defined 'shoulder' region near 1 mm and curving convex downwards for larger sizes. Able and Boutle (2012) also found that the exponential function provided a good fit to their data for the precipitation mode (also consistent with visual inspection of our combined spectra). It is worth mentioning that their data were acquired with aircraft-mounted 2D-Cloud and 2D-Particle probes in oceanic warm rain cumulus clouds. The precipitation that was observed during the event in Huntsville was similar in that it was largely dominated by warm rain processes and characterized by relatively weak rainfall rates. Furthermore, the shape of the combined MPS-2DVD DSDs, especially during the Huntsville event, resembles that of the bi-modal DSDs produced by simulations of raindrop collisions (e.g., McFarquahar 2004; Straub et al. 2010). This suggests that collision-induced breakups were responsible for shaping the observed shoulder region, which was more prominent in the Huntsville warm rain event and during times of thunderstorms observed in the Greeley campaign.

Time integration of the spectra over 1-2 h clearly brings out the systematic differences when comparing 2DVD-only and the combined MPS-2DVD spectra. The combined spectra indicate that a gamma model could not possibly fit the entire size range at either of the two climatologically different sites. However, the gamma model with parameters ($N_W$, $D_m$, $\mu$; Illingworth and Blackman 2002; Testud et al. 2001) has been used to describe the shape of the aforementioned precipitation mode of the spectrum using data from 2DVD primarily for radar applications (e.g., Bringi et al. 2003; Brandes et al. 2002; Williams et al. 2014). The fitted $\mu$ -values showed a broad distribution with mean values between 3-5. To better characterize the small drop end, Thurai et al (2014) describe the use of single camera data (from 2DVD; using the same methodology as the MPS except for poorer resolution) to re-adjust the standard 2DVD-derived concentrations for $D < 0.6$ mm. After such adjustment, the fitted $\mu$ values were found to be significantly lower ($\mu$ between -2 to 2) when compared with the much larger and positive $\mu$-values for non-adjusted DSDs. One of the example cases was a light precipitation event in Emasalo, Finland, where the adjusted 2DVD-based DSDs had been compared to the DSD measurements made with the high resolution (25 μm) Cloud Imaging Probe on the Wyoming King Air aircraft (during a spiral descent over the 2DVD). The 2DVD-adjusted concentrations were found to be in good agreement with the airborne data for small drops. Both showed much higher concentrations of small drops, similar to the drizzle mode found with the MPS measurements both in Greeley and Huntsville, as well as those given in Abel and Boutle (2012).

Our new observations also point out that the earlier studies conclusions (e.g.Willis, 1984; Ulbrich, 1985; Vivekanandan et al., 2004) regarding truncation errors for gamma model DSD's may no longer hold for some integral parameters, especially those related to the lower order moments and shape (or breadth) of the DSD. Furthermore, it may be that if a mathematical model is required to represent the entire DSD, then a single gammal model with a triplet of parameters may not be sufficient to fully represent the DSD for these properties. It may be necessary to consider other models, including mixed models where one model is used for the drizzle mode and another for the precipitation mode. This points to the potential need for additional work on modeling DSD's across the full spectrum of measured drops sizes and to assessing errors associated with those new models. Another, more attractive, formulation is the generalized gamma function, as considered for example by Auf der Maur, 2001, and later by Lee et al., 2004 who have illustrated a sample of possible shapes that can be represented by this function. The flexibility of this method may well be suitable for describing the full DSD spectra reported in this paper.

*b) Polarimetric radar retrievals*

As we saw earlier in sections 3 and 4, the higher concentration of small drops results in lower $D_m$ and higher $\sigma_M$. This has two implications. Firstly, the variation of $D_m$ with $Z_{dr}$ will be different (i.e., for a given radar measured $Z_{dr}$, the $D_m$ values are slightly lower for the combined spectra) but as indicated by the Greeley results, this negative bias in $D_m$ becomes more significant for low rainfall rates. The second implication is that the $\sigma_M$ versus $D_m$ variation is significantly modified when the more accurate small drop concentrations are included in the DSDs. More importantly, the ratio $\sigma_M/D_m$ becomes amplified due to the combined effects of increase in $\sigma_M$ along with a decrease in $D_m$ for the combined spectra. Since for a gamma model $\sigma_M/D_m=(4+\mu)^{-1/2}$ it follows that the "effective" μ will be significantly reduced for the combined spectra (the notion of "effective" μ is introduced since the combined spectra in general would not follow the gamma model, and as mentioned earlier, a better representation would be the generalized gamma function). This amplification of $\sigma_M/D_m$ is similar to truncating the spectra at the small drop end due to instrument limitations (Ulbrich and Atlas 1998). Our combined spectra results suggest that polarimetric or dual frequency retrieval algorithms that assume a constant μ value (typically $\mu\approx3$) or a μ-Λ relation (Λ is the slope factor in the gamma model, e.g., $\Lambda D_m=4+\mu$) or use the ratio $\sigma_M$/Dm to estimate μ statistically (e.g., Kozu et al., 2009; Zhang et al., 2003; Williams et al., 2014), may need further evaluation. Note these are some of the assumptions which are used for the DSD retrievals from the GPM Dual-frequency Precipitation Radar (DPR; Hou et al., 2014, Munchak and Tokay, 2008). Finally, whereas it is self-evident that the total number concentration will be much higher for the combined spectra relative to the 2DVD-only case, the normalized intercept parameter $N_W$ being proportional to $W/D_m^4$ will also be amplified due to the $D_m$ being raised to the 4th power.

In the past, the estimation of $D_m$ from S-band polarimetric radar has only used $Z_{dr}$. Our results from the Greeley campaign show that for low rainfall rates the S-band $Z_{dr}$ becomes insensitive to DSD because it is more dominated by small drops, which tend to be more spherical. In particular, for DSDs with $D_m$ < 1 mm, the CHILL S-band $Z_{dr}$ was nearly 0 dB whereas $Z_h$ showed more noticeable variation with $D_m$. For DSDs with $D_m$ < 1 mm $Z_{dr}$, which was around 0 dB (see Fig. 9a), does not seem to provide any useful information to retrieve the small end of the drop size spectrum. Hence, a formula combining both parameters would be more appropriate for $D_m$ estimation. This would be particularly applicable for rain regimes which are dominated by small drops, even at high rain rates, such as hurricane systems (e.g., Tokay et al. 2008, Brown et al., 2016) as well as warm shallow rain in sub-tropical (e.g., Thurai and Bringi 2008) and tropical oceanic locations (Thompson et al. 2015).

### *c) GPM DPR retrieval algorithm*

The $\sigma_M$ variation with $D_m$ can be useful for the satellite-radar based estimates of rainfall rates at ground level. Specifically, the GPM DPR needs to make assumptions on the shape of the DSD in order to retrieve DSD parameters such as $D_m$ and $N_W$ (Iguchi et al. 2016). These findings, along with our modified $\sigma_M$ versus $D_m$ variation, suggest that a variable (or more flexible) $\mu$ - $D_m$ relationships be used in the satellite retrieval of the DSD parameters (if indeed gamma DSD is assumed, rather than generalized gamma, as mentioned earlier). However, an initial assessment of the DPR performance indicates the retrievals discussed above for the Huntsville event agree within the limits of uncertainty. Preliminary comparisons between 2ADPR and GPM Ground Validation Network (VN) DSDs, which rely on ground-based polarimetric radar data (e.g., WSR-88DP) to estimate $D_m$, suggest that the DPR and VN $D_m$'s associated with stratiform precipitation are quite similar. The DPR estimates being biased only 0.1 mm high relative to VN estimates. The mean absolute error of the DPR Dm retrievals relative to the ground radar retrievals is 0.2 mm. Hence, the DPR retrieved $D_m$ (1.8 mm) for this Huntsville event compares rather well with the combined MPS-2DVD measurement of $D_m$ (1.6 mm), at least within the uncertainty of the 2ADPR Dm retrieval.

## 6. Summary

Two collocated disdrometers have been used to measure the full drop size distribution with high resolution (50 μm) for small drops (MPS) and good resolution (170 μm) for moderate to large drops (2DVD) in two spring-time rain events occurring in widely different climatologies. After time integration of 1-2 h, the 2DVD-based spectra were found to systematically underestimate the concentrations at the small drop end relative to the MPS-based spectra. There was very good agreement in the overlapping size interval between the two instruments giving confidence in the interpretation of the combined spectra in terms of physical processes as opposed to instrument-to-instrument differences. Examination of the combined spectra revealed a drizzle mode for D<~0.7 mm and a precipitation mode for larger diameters in agreement with the identification of such modes by Able and Boutle (2012) which was based on using aircraft imaging probes (2D-C and 2D-P) in warm rain oceanic clouds. While the two events analyzed herein were from different regions (Greeley, CO and Hunstville, AL), the two modes could be easily identified in the combined spectra (largely independent of rain rate). However, no attempt is made here to suggest physical processes giving rise to the two modes other than the general domination of ice-phase microphysics in the Greeley event and warm cloud base convection with component of warm rain microphysics in the Huntsville event, with negligible evidence of evaporation causing a depletion of tiny drops at either location as inferred from the presence of the drizzle mode throughout the duration of the precipitation events.

The 1-min averaged combined spectra were also analyzed in terms of the parameters $N_W$, $D_m$ and $\sigma_M$ which are relevant for radar applications (based on both polarimetric and dual-frequency). Note that these three parameters are defined in terms of higher order moments of the spectra (3rd moment and/or higher moments) with no assumption of the gamma DSD model (Haddad et al,. 1996, Ulbrich and Atlas, 1998, Testud et al. 2001). While all three parameters are affected by the small drop concentrations especially at light rain rates, the $N_W$ and the ratio $\sigma_M/D_m$ were found to be significantly affected (significantly larger) by the small drop concentrations in the drizzle mode even at high rain rates in the two events analyzed herein. This result is particularly relevant for radar-based retrievals which assume the gamma model (the parameters being $N_W$, $D_m$ and the shape $\mu$) with the $\mu$ parameter being fixed ($\approx 3$) or based on $D_m$. The general tendency (under such assumptions) is for the radar retrievals to overestimate $D_m$ and underestimate $N_W$. Clearly, more data with the combined MPS-2DVD instruments are needed in a variety of rain rates and different climatologies to improve the radar-based retrievals. Such datasets should also impact the numerical modeling of the microphysics of rain processes which use multi-moment bulk schemes (here the total number concentration is of primary importance and it is obvious that the drizzle mode in the combined DSD would play a significant role).

For each of the two events analyzed, we also had available polarimetric radar data and were able to characterize the variation of radar measured $Z_{dr}$ (and $Z_h$) with $D_m$ from the combined spectra. In the Greeley event, this variation was well-captured at the small values of $D_m$ (< 0.5 mm) where measured $Z_{dr}$ tended to 0 dB which precluded the estimation of $D_m$ based on $Z_{dr}$ alone. A retrieval of $D_m$ using both $Z_h$ and $Z_{dr}$ would be more appropriate but will be addressed as more combined datasets become available in the future.

The small raindrop findings presented here also have implications for satellite-based retrieval of DSD parameters and ultimately surface rainfall rates. An overpass of the GPM DPR during an event of the Huntsville campaign revealed that the DPR algorithm overestimated $D_m$ and underestimated $N_w$ relative to the combined MPS-2DVD measurements. This indicates that a fixed $\mu$ in the gamma distribution may not be the most fitting assumption to describe the DSD from a satellite-based radar perspective. Instead, the above $\sigma_M$-$D_m$ relationship, which for application purposes needs to be converted into $\mu$-$D_m$ space (e.g., Williams et al. 2014), could facilitate more accurate retrievals. However, this speculation requires further investigation since unlike Williams et al. (2014), we did not account for any correlation that might exist between $\sigma_M$ and $D_m$ calculated from the combined MPS-2DVD measurements before fitting a power-law.

Although only two events are reported in this paper, analyses of several other events have also shown that the full DSD spectra has the aforementioned drizzle mode and the precipitation mode which together could be better represented by the use of generalized gamma function (Auf Der Maur, 2001, Lee et al. 2004).

***Acknowledgments*:** MT, VNB and BN acknowledge support by the National Science Foundation under grant AGS-1431127. Additionally MT acknowledges support from NASA's Global Precipitation Measurement program through award NNX16AD47G. We also wish to thank Matt Freer of Droplet Measurement Technologies, Boulder, Colorado, for giving advice on MPS data processing, and Dave Marks (NASA-Wallops) for producing the image of GPM DPR swath across northern Alabama during the 11 April 2016 event, from the 2ADPR product.

# Appendix

Calculation of DSDs from the 2DVD data is a very well established procedure and hence only the calculation of DSDs from the MPS data is summarized here. This involves the sample area calculation which is described in the MPS data analysis guide by Droplet Measurement Technologies. It first entails the calculation of the effective array width *(EAW)* and the depth of field *(DoF)*.

$$EAW = R_p * (n - x - 1) \quad \text{(A1)}$$

where $R_p$ is the probe resolution, $n$ is number of diodes (= 64) and $x$ is the bin number (1:62), and

$$DoF = 6\, r^2 / \lambda \quad \text{(A2)}$$

where $r$ is the particle radius and $\lambda$ is the laser wavelength, all in MKS units.

The DSD denoted by $N(D)$ is then given by:

$$N(D) = C / (Aeff * v * \Delta t * \Delta d) \quad \text{(A3)}$$

where $C$ is the number of particles measured in the diameter interval $\Delta d$, and $\Delta t$ is the time interval and $v$ represents the particle velocity, and $A_{eff}$ is the effective area given by:

$$A_{eff} = EAW * DoF \quad \text{(A4)}$$

Note although the MPS measures the velocity of each particle, in our DSD calculations, we have used a recommended velocity-diameter relationship for small drops:

$$v = -19.27 + (0.50*D_\mu) - (9.04*1e\text{-}5*D_\mu^2) + (5.66*1e\text{-}9*D_\mu^3) \quad \text{(A5)}$$

which yields $v$ in cm/s at sea level and requires a suitable correction factor for high altitudes such as Greeley, and $D_\mu$ is $D_{eq}$ in microns. Eq. (A5) yields similar values to the Gunn-Kinzer (1949) data for drops smaller than 1.2 mm.

## REFERENCES


Abel, S. J. and Boutle, I. A., 2012: An improved representation of the rain size spectra for single-moment microphysics schemes. *Q. J. Royal Meteorol. Soc.*, **138** (669), 2151–2162, DOI: 10.1002/qj.1949.

Atlas, D., R. C. Srivastava, and R. S. Sekhon, 1973: Doppler radar characteristics of precipitation at vertical incidence. *Rev. Geophys*., **11**, 1–35.

Auf Der Maur, A. N., 2001: Statistical Tools for Drop Size Distributions: Moments and Generalized Gamma. *J. Atmos. Sci.*, **58**, 407-418. 11th Conference on Cloud Physics, paper 8.6, Ogden, Utah.

Belda M, E. Holtanová, T. Halenka, J. Kalvová. 2014: Climate classification revisited: from Köppen to Trewartha. Clim. Res. 59: 1–13, doi: 10.3354/cr01204.

Baumgardner, D., G. Kok, W. Dawson, D. O’Connor and R. Newton, 2002: A New Groundbased Precipitation Spectrometer: The Meteorological Particle Sensor (MPS), 11th Conference on Cloud Physics, 3-7 June 2002, Ogden, Utah.

Beard, K. V., and A. R. Jameson, 1983: Raindrop canting, *Journal of the Atmospheric Sciences*, **40**, 448-454.

Brandes, E. A., G. Zhang, and J. Vivekanandan, 2002: Experiments in Rainfall Estimation with a Polarimetric Radar in a Subtropical Environment, *Journal of Applied Meteorology*, **41**, 674–685.

Bringi, V. N., V. Chandrasekar, J. Hubbert, E. Gorgucci, W. L. Randeu, and M. Schoenhuber, 2003: Raindrop size distribution in different climatic regimes from disdrometer and dual-polarized radar analysis. *J. Atmos. Sci.*, **60**, 354–365.

Bringi, V. N., R. Hoferer, D. A. Brunkow, R. Schwerdtfeger, V. Chandrasekar, S. A. Rutledge, J. George, P. C. Kennedy, 2011: Design and Performance Characteristics of the New 8.5-m Dual-Offset Gregorian Antenna for the CSU–CHILL Radar, *Journal of Atmospheric and Oceanic Technology*, **28**, 907–920.

Brown, B. R., Bell, M. M., and Frambach, A. J., 2016, Validation of simulated hurricane drop size distributions using polarimetric radar, *Geophysical Research Letters*, **43,** 910–917.

Gatlin, P. N., M. Thurai, V. N. Bringi, W. Petersen, D. Wolff, A. Tokay, L. Carey, M. Wingo, 2015: Searching for Large Raindrops: A Global Summary of Two-Dimensional Video Disdrometer Observations. *J. Appl. Meteor. Climatol.*, **54**, 1069–1089.

Gunn, K. L. S., and G. D. Kinzer, 1949: The terminal velocity of fall for water droplets in stagnant air. *J. Meteor.*, **6**, 243–248.

Haddad, Z. S., S. L. Durden, and E. Im, 1996: Parameterizing the raindrop size distribution. *J. Appl. Meteor.*, **35**, 3–13.

Heymsfield, A. J., and J. L. Parrish, 1978: A Computational Technique for Increasing the Effective Sampling Volume of the PMS Two-Dimensional Particle Size Spectrometer. *J. Appl. Meteor.*, **17**, 1566–1572.

Hou, A. Y., R. K. Kakar, S. Neeck, A. A. Azarbarzin, C. D. Kummerow, M. Kojima, R. Oki, K. Nakamura, and T. Iguchi, 2014: The Global Precipitation Measurement Mission, *Bulletin of the American Meteorological Society*, **95** (5), 701–722.

Iguchi, T., S. Seto, R. Meneghini, N. Yoshida, J. Awaka, M. Le, V. Chandrasekar, T. Kubota, 2016: GPM/DPR Level-2 Algorithm Theoretical Basis Document (ATDB), Version 4.0. [Available at https://pps.gsfc.nasa.gov/atbd.html].

Illingworth, A. J., and T. M. Blackman, 2002: The need to represent raindrop size spectra as normalized gamma distributions for the interpretation of polarization radar observations. *J. Appl. Meteor.*, **41**, 286–297.

Johnson, D. B., and K. V. Beard, 1984: Oscillation Energies of Colliding Raindrops. *J. Atmos. Sci.*, **41**, 1235–1241.

Knollenberg, R. G., 1970: The optical array: An alternative to scattering and extinction for airborne particle size determination, *J. Appl. Met.*, **9**, 86-103.

Kozu, T., T. Iguchi, T. Kubota, N. Yoshida, S. Seto, J. Kwiatkowski, and Y. Takayabu, 2009: Feasibility of raindrop size distribution parameter estimation with TRMM precipitation radar. *J. Meteor. Soc. Japan*, **87A**, 53–66.

Krajewski, W. F., A. Kruger, C. Caracciolo, P. Golé, L. Barthes, J-D Creutin, J-Y Delahaye, E. I. Nikolopoulos, F. Ogden, J-P Vinson, 2006: DEVEX-disdrometer evaluation experiment: Basic results and implications for hydrologic studies, *Advances in Water Resources*, **29**, 311–325.

Kruger, A., and W. F. Krajewski, 2002: Two-dimensional video disdrometer: A description. *J. Atmos. Oceanic Technol.*, **19**, 602–617.

Lee, G., I. Zawadzki, W. Szyrmer, D. Sempere-Torres, and R. Uijlenhoet, 2004: A General Approach to Double-Moment Normalization of Drop Size Distributions, *Journal of Applied Meteorology*, **43**, 264–281.

Löffler-Mang, M., and J. Joss, 2000: An optical disdrometer for measuring size and velocity of hydrometeors. *J. Atmos. Oceanic Technol.*, **17**, 130–139.

McFarquhar, G. M., 2004: A new representation of collision-induced breakup of raindrops and its implications for the shapes of raindrop size distributions. *J. Atmos. Sci.*, **61**, 777–794.

Meyers, M. P., R. L. Walko, J. Y. Harrington, and W. R. Cotton, 1997: New RAMS cloud microphysics. Part II: The two-moment scheme. *Atmos. Res.*, **45**, 3–39.

Milbrandt, J. A., M. K. Yau, 2005: A Multimoment Bulk Microphysics Parameterization. Part I: Analysis of the Role of the Spectral Shape Parameter. *J. Atmos. Sci.*, **62**, 3051–3064.

Miriovsky, B. J. and Coauthors, 2004: An experimental study of small-scale variability of radar reflectivity using disdrometer observations. *J. Appl. Meteorol.*, **43**, 106-118.

Montero-Martinez, G., A. B. Kostinski, R. A. Shaw, and F. Garcia-Garcia, 2009: Do all raindrops fall at terminal speed?, *Geophys. Res. Lett.*, **36**, L11818

Munchak, S. P., and A. Tokay, 2008: Retrieval of raindrop size distribution from simulated dual-frequency radar measurements. *J. Appl. Meteor. Climatol.*, **47**, 223–239.

Notaroš B. M., V. N. Bringi, C. Kleinkort, P. Kennedy, G-J Huang, M. Thurai, A. J. Newman, W. Bang and G. Lee, 2016: Accurate Characterization of Winter Precipitation Using Multi-Angle Snowflake Camera, Visual Hull, Advanced Scattering Methods and Polarimetric Radar, *Atmosphere*, **7**(6), 81; doi:10.3390/atmos7060081

OTT Messtechnik GmbH, 2010: Operating instructions Precipitation Gauge OTT Pluvio.

Petersen, W. A., K. R. Knupp, D. J. Cecil, and J. R. Mecikalski, 2007: The University of Alabama Huntsville THOR Center instrumentation: Research and operational collaboration, Preprints, 33rd Int. Conf. on Radar Meteorology, Cairns, Australia, Amer. Meteor. Soc., 5.1. [Available online at https://ams.confex.com/ams/33Radar/webprogram/Paper123410.html.]

Sempere Torresa, D., J. M. Porrà, and J-D Creutin, 1994: A General Formulation for Raindrop Size Distribution, *Journal of Applied Meteorology*, **33**, 1494–1502.

Shönhuber, M., G. Lammar and W. L. Randeu, 2008: "The 2D-video-vistrometer", Chapter 1 in "*Precipitation: Advances in Measurement, Estimation and Prediction*", Michaelides, Silas. (Ed.), Springer, ISBN: 978-3-540-77654-3.

Straub, W., K. D. Beheng, A. Seifert, J. Schlottke, and B. Weigand, 2010: Numerical investigation of collision-induced breakup of raindrops. Part II: Parameterizations of coalescence efficiencies and fragment size distributions. *J. Atmos. Sci.*, **67**, 576–588.

Testud, J., S. Oury, R. A. Black, P. Amayenc, and X. K. Dou, 2001: The concept of "normalized" distribution to describe raindrop spectra: A tool for cloud physics and cloud remote sensing. *J. Appl. Meteor.*, **40**, 1118–1140.

Thompson, E. J., S. A. Rutledge, B. Dolan, and M. Thurai, 2015: Drop Size Distributions and Radar Observations of Convective and Stratiform Rain over the Equatorial Indian and West Pacific Oceans, *Journal of the Atmospheric Sciences*, **72**, 4091–4125.

Thurai, M., and V. N. Bringi, 2005: Drop axis ratios from a 2D video disdrometer. *J. Atmos. Oceanic Technol.*, **22**, 966–978.

Thurai M. and V. N. Bringi, 2008: Rain microstructure from polarimetric radar and advanced disdrometers, Chapter 10 in *Precipitation: Advances in Measurement, Estimation and Prediction,* S. C. Michaelides, Ed., Springer, ISBN: 978-3-540-77654-3.

Thurai, M., V.N. Bringi, L. D. Carey, P. Gatlin, E. Schultz and W.A. Petersen, 2012: Estimating the accuracy of polarimetric radar-based retrievals of drop size distribution parameters and rain rate: An application of error variance separation using radar-derived spatial correlations. *J. Hydrometeor*, **13**, 1066–1079.

Thurai, M., C.R. Williams, and V.N. Bringi, 2014: Examining the correlations between drop size distribution parameters using data from two side-by-side 2D-video disdrometers. *Atmospheric Research*, **144**, 95-110.

Thurai, M., V. N. Bringi, P. C. Kennedy, B. Notaroš, and P. N. Gatlin, 2015: Towards Completing the Rain Drop Size Distribution Spectrum: A Case Study Involving 2D Video Disdrometer, Droplet Spectrometer, and Polarimetric Radar Measurements in Greeley, Colorado, Proceedings of the 37th AMS Conference on Radar Meteorology, Norman, Oklahoma, USA. Sept. 2015, Paper 4B.1 (Extended Abstract available online at: https://ams.confex.com/ams/37RADAR/webprogram/Paper275321.html).

Tokay, A., A. Kruger, and W. F. Krajewski, 2001: Comparison of drop Size distribution measurements by impact and optical disdrometers. *J. Appl. Meteor.*, **40**, 2083–2097.

Tokay, A., P.G. Bashor, E. Habib, and T. Kasparis, 2008: Raindrop Size Distribution Measurements in Tropical Cyclones. *Mon. Wea. Rev.*, **136**, 1669–1685.

Trewartha, G.T. and L.H. Horn, 1980: Introduction to climate, 5th edition. McGraw Hill, New York, NY.

Ulbrich, C. W., 1983: Natural Variations in the Analytical Form of the Raindrop Size Distribution, *J. of Clim. and Appl. Meteorol.*, **22**, 1764–1775.

Ulbrich, C. W., and D. Atlas, 1998: Rain microphysics and radar properties: Analysis methods for drop size spectra. *J. Appl. Meteor.*, **37**, 912–923,

Vivekanandan, J., G. Zhang, and E. Brandes, 2004: Polarimetric radar estimators based on a constrained gamma drop size distribution model. J. Appl. Meteor., 43, 217–230.

Williams, C.R., V. N. Bringi, L. D. Carey, V. Chandrasekar, P. N. Gatlin, Z. S. Haddad, R. Meneghini, S. J. Munchak, S. W. Nesbitt, W. A. Petersen, S. Tanelli, A. Tokay, A. Wilson, and D. B. Wolff, 2014: Describing the Shape of Raindrop Size Distributions Using Uncorrelated

Raindrop Mass Spectrum Parameters, *Journal of Applied Meteorology and Climatology*, **53**, 1282–1296.

Willis, P. T. 1984. Functional fits to some observed drop size distributions and parameterization of rain. J. Atmos. Sci. 41:1648–1661.

Zhang, G., J. Vivekanandan, E. A. Brandes, R. Meneghini, and T. Kozu, 2003: The shape–slope relation in observed gamma raindrop size distributions: Statistical error or useful information? *J. Atmos. Oceanic Technol.*, **20**, 1106–1119,

## FIGURE CAPTIONS

FIG. 1: (a) The MPS, 2DVD and Pluvio inside the double wind fence at the site near Greeley, Colorado (40.3273569N, 104.6093944W, 1.4 km AMSL). (b) MPS, 2DVD and Parsivel disdrometers inside the double wind fence at the Huntsville site (34.7233333N, 86.6419444W, 212 m AMSL).

FIG. 2: (a): Picture of a Meteorological Particle Spectrometer and the custom-design stand. A wind vane aligns the sample path with the wind flow but was not used in our campaigns since the instrument was installed within a DFIR. (b): schematic of a drop falling through the MPS sensor measurement area; There are 64 photo-detectors and the horizontal resolution is 50 µm. From Droplet Measurement Technologies (DMT).

FIG. 3: (a) Fall velocity versus drop equi-volume diameter ($D_{eq}$) from the 2DVD data as 2D frequency of occurrence plot. The dashed line represents the equation given in Atlas et al. (1973) that approximates the Gunn-Kinzer terminal fall speed measurements (Gunn and Kinzer 1949), and the dotted line is this approximation after applying altitude correction for the 1.4 km AMSL for Greeley. (b) Velocity of histograms specific to all drops with $D_{eq}$ values of 2.5 ± 0.1 mm. The expected values at sea level (7.3 m/s) and at 1.4 km altitude (7.9 m/s) are shown as dashed line and dot-dash line respectively.

FIG. 4: (a) 1-minute rain-rate (R) from Pluvio for the entire event; (b) the corresponding rain accumulation; (c) the corresponding 2-hour rain accumulations.

FIG. 5: 2-hour DSD comparisons from the 2DVD (crosses) and 2DVD-MPS combined (diamonds) for the 17 April 2015 event. The time interval is specified for each case. Note log-log scale is used to focus on the small drops.

FIG. 6: (a) $D_m$ derived from 1 minute DSDs using 2DVD data (grey points), and the combined MPS-2DVD data (black points); (b) the corresponding $\sigma_M$ values; (c) the $\sigma_M$ - $D_m$ scatter plot using the same DSDs and their fitted curves for $D_m \geq 0.5$ mm. 3-minute smoothing is applied to (a) and (b) in order to show more clearly the differences in grey and the black points.

FIG. 7: $D_m$ histogram comparisons for three different rain types (as indicated in the top panels) and for different rainfall rate intervals (as indicated in bottom panels). The 2DVD data-based histograms are shown in grey and the combined MPS-2DVD DSD based histograms are shown in black. All histograms are based on 1-minute DSDs.

FIG. 8: $D_m$ comparisons between 2DVD-based and 2DVD-MPS combined DSD based estimates. Each data point is based on 1-min spectra.

FIG. 9: (a) the CHILL S-band $Z_{dr}$ and (b) the CHILL S-band $Z_h$ measurements over the instrument site versus $D_m$ calculated using 2DVD (grey) and MPS-2DVD combined DSDs (black).

FIG. 10: (a) Fall velocity versus drop $D_{eq}$ from the 2DVD data as 2D frequency of occurrence plot. The dashed line represents the equation given in Atlas et al. (1973) which represents the Gunn-Kinzer variation, (b) histogram of vertical velocity specific to all drops with $D_{eq}$ values of 2.5 ± 0.1 mm. The expected value at sea level (7.3 m/s) is shown as dot-dash line.

FIG. 11: Hourly DSD comparisons from the 2DVD (crosses) and 2DVD-MPS combined (diamonds) for the 11 April 2016 event in Huntsville. The time interval is specified for each case. The hourly rain accumulations were 1.3, 2.3, 1.6, 4.1, 4.4, and 3.7 mm for the 17, 18, 19, 20, 21, 22 hr UTC respectively.

FIG. 12: (a) $D_m$ derived from 1 minute DSDs (after smoothing over 3 minutes) using 2DVD data alone (grey circles), and the combined MPS-2DVD data (black crosses); (b) the corresponding $\sigma_M$ values; (c) the corresponding $\log_{10}$ ($N_W$).

FIG. 13: (a) dBZ extracted over the MPS-2DVD site from the C-band ARMOR radar; (b) the corresponding $Z_{dr}$ (black crosses) and values of $D_m$ derived from the combined DSDs; (c) variation of the C-band $Z_{dr}$ with $D_m$ values from the 2DVD DSDs (grey) and the combined DSDs (black). Note that some of the scatter is due to radar measurement error.

FIG. 14: The GPM DPR swath across northern Alabama during the 11 April, 2016 event showing a) $D_m$ [mm] and b) $10.\log_{10}(N_W)$ [$m^{-3}mm^{-1}$] both at 500-m AGL from the 2ADPR product, and (c) the 10-minute DSD from 23:25 – 23:35 UTC, from the MPS and 2DVD around the GPM overpass time period, at 23:31 UTC..

**(a)**

**(b)**

FIG. 1: (a) The MPS, 2DVD and Pluvio inside the double wind fence at the site near Greeley, Colorado (40.3273569N, 104.6093944W, 1.4 km AMSL). (b) MPS, 2DVD and Parsivel disdrometers inside the double wind fence at the Huntsville site (34.7233333N, 86.6419444W, 212 m AMSL).

**(a)** **(b)**

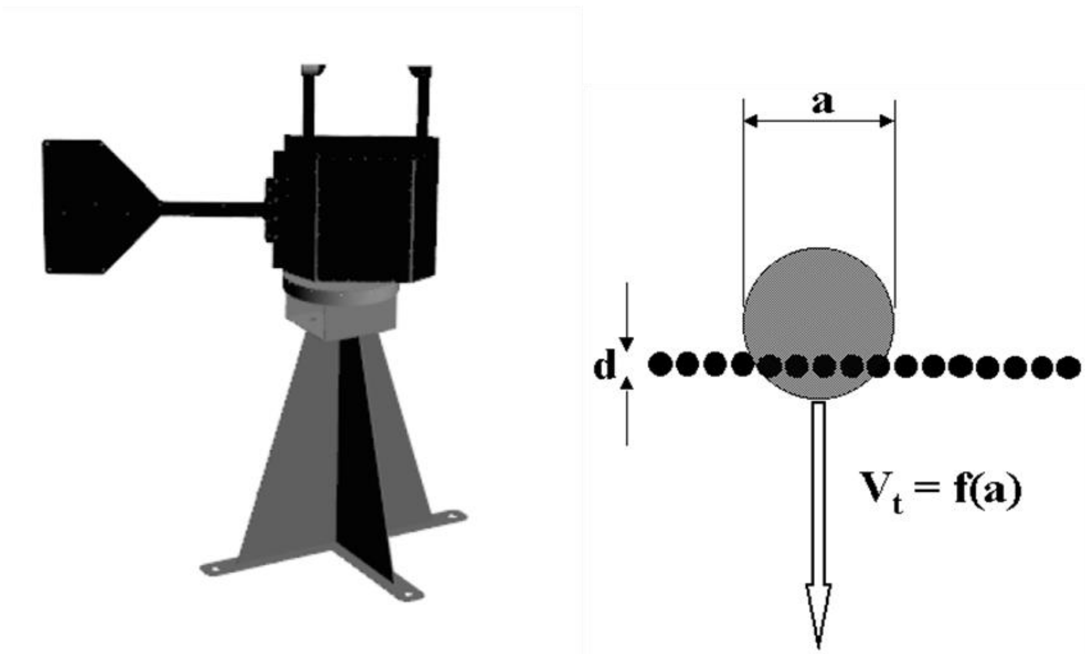


FIG. 2: (a): Picture of a Meteorological Particle Spectrometer and the custom-design stand. A wind vane aligns the sample path with the wind flow but was not used in our campaigns since the instrument was installed within a DFIR. (b): schematic of a drop falling through the MPS sensor measurement area; There are 64 photo-detectors and the horizontal resolution is 50 µm. From Droplet Measurement Technologies (DMT).

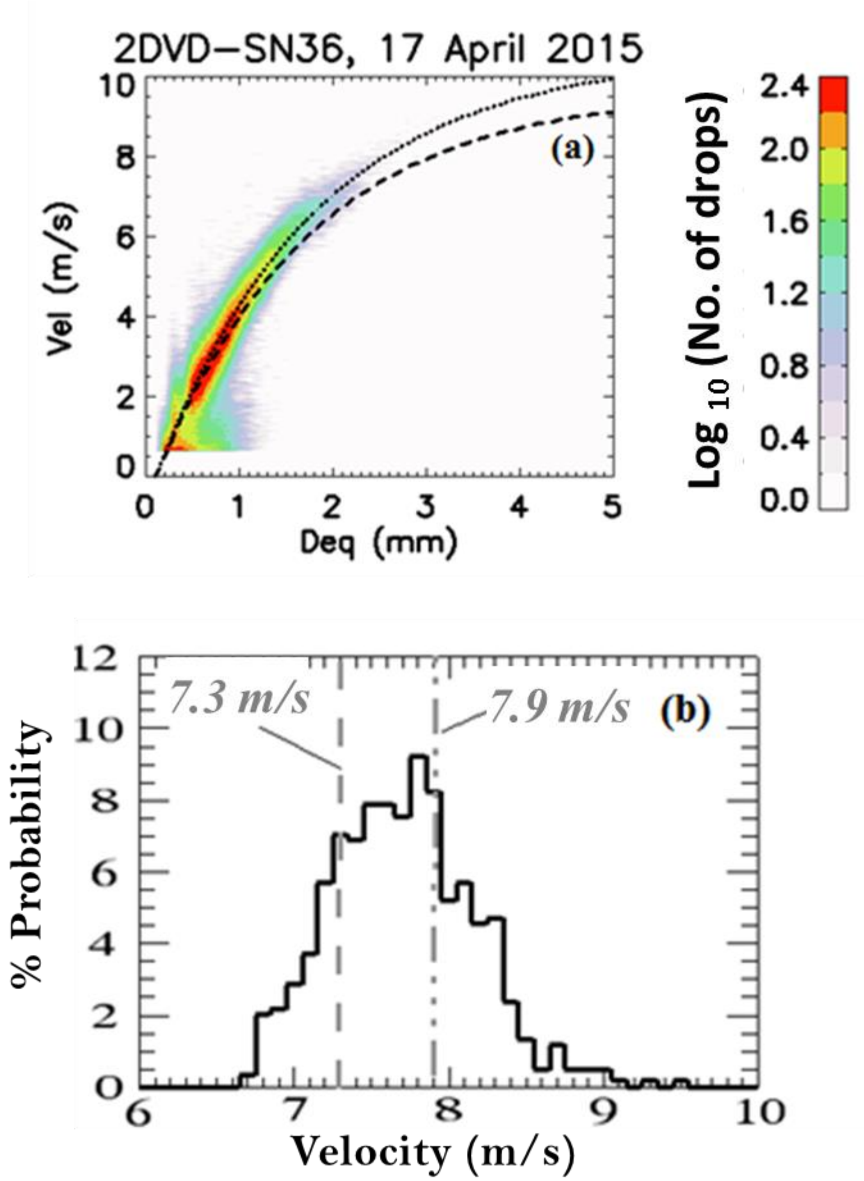


FIG. 3: (a) Fall velocity versus drop equi-volume diameter ($D_{eq}$) from the 2DVD data as 2D frequency of occurrence plot. The dashed line represents the equation given in Atlas et al. (1973) that approximates the Gunn-Kinzer terminal fall speed measurements (Gunn and Kinzer 1949), and the dotted line is this approximation after applying altitude correction for the 1.4 km AMSL for Greeley. (b) Velocity of histograms specific to all drops with $D_{eq}$ values of 2.5 ± 0.1 mm. The expected values at sea level (7.3 m/s) and at 1.4 km altitude (7.9 m/s) are shown as dashed line and dot-dash line respectively.

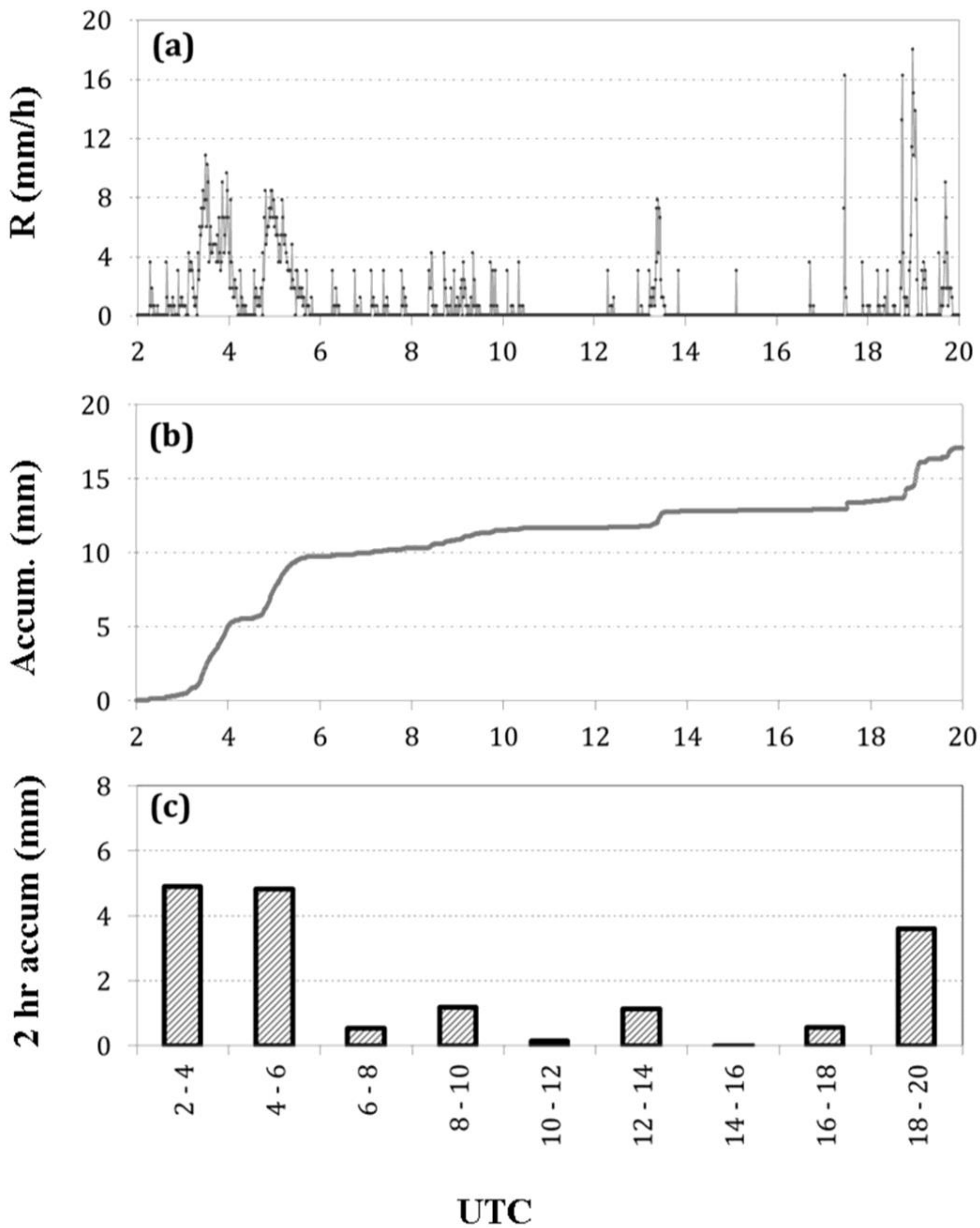


FIG. 4: (a) 1-minute rain-rate (R) from Pluvio for the entire event; (b) the corresponding rain accumulation; (c) the corresponding 2-hour rain accumulations.

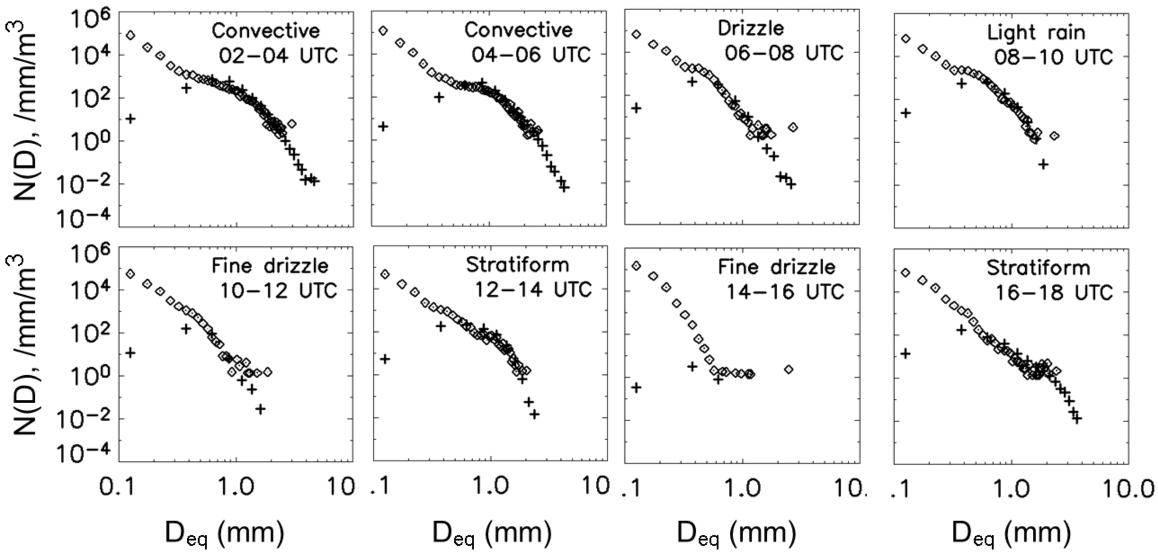


FIG. 5: 2-hour DSD comparisons from the 2DVD (crosses) and 2DVD-MPS combined (diamonds) for the 17 April 2015 event. The time interval is specified for each case. Note log-log scale is used to focus on the small drops.

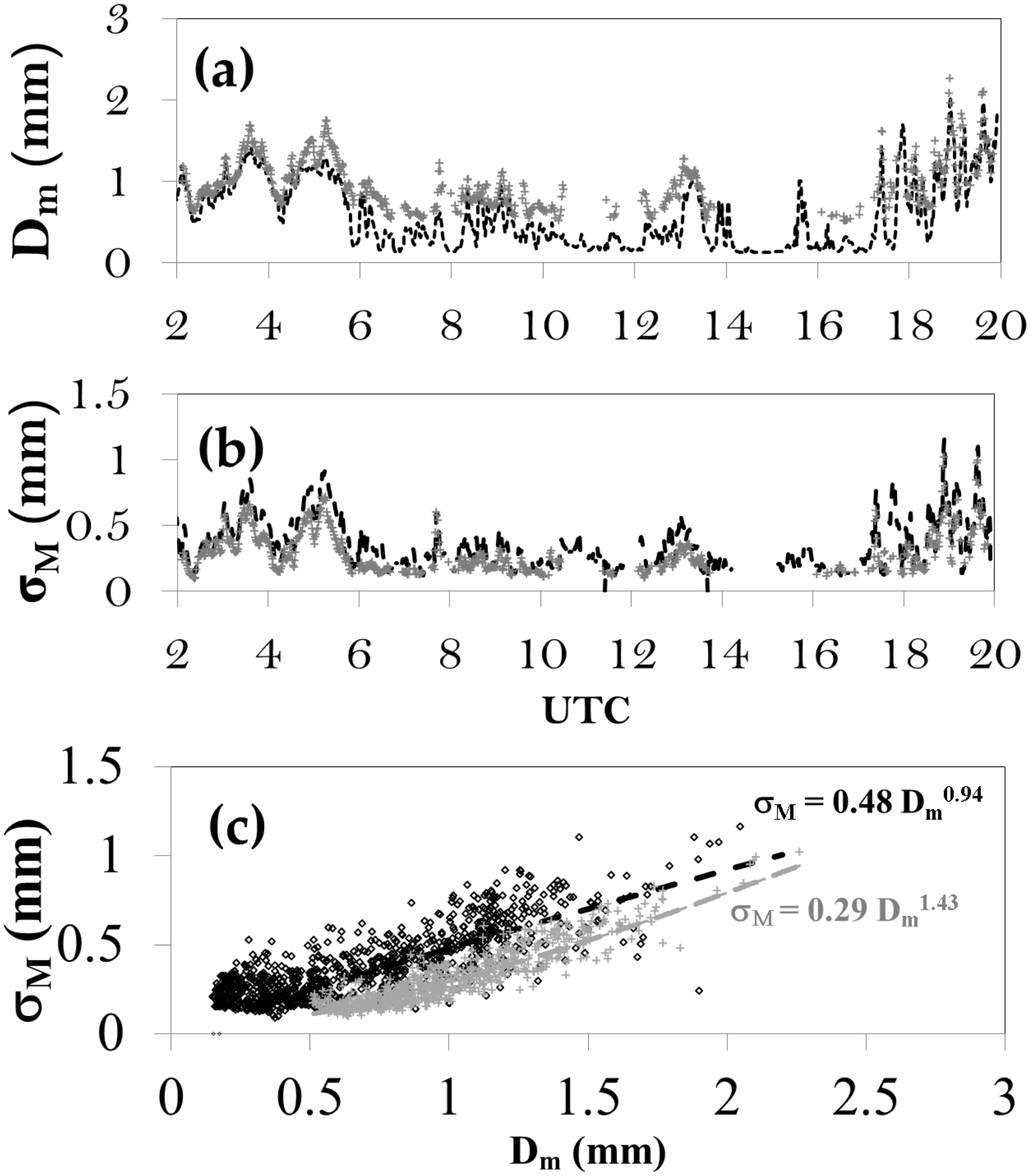


FIG. 6: (a) $D_m$ derived from 1 minute DSDs using 2DVD data (grey points), and the combined MPS-2DVD data (black points); (b) the corresponding $\sigma_M$ values; (c) the $\sigma_M$ - $D_m$ scatter plot using the same DSDs and their fitted curves for $D_m \geq 0.5$ mm. 3-minute smoothing is applied to (a) and (b) in order to show more clearly the differences in grey and the black points.

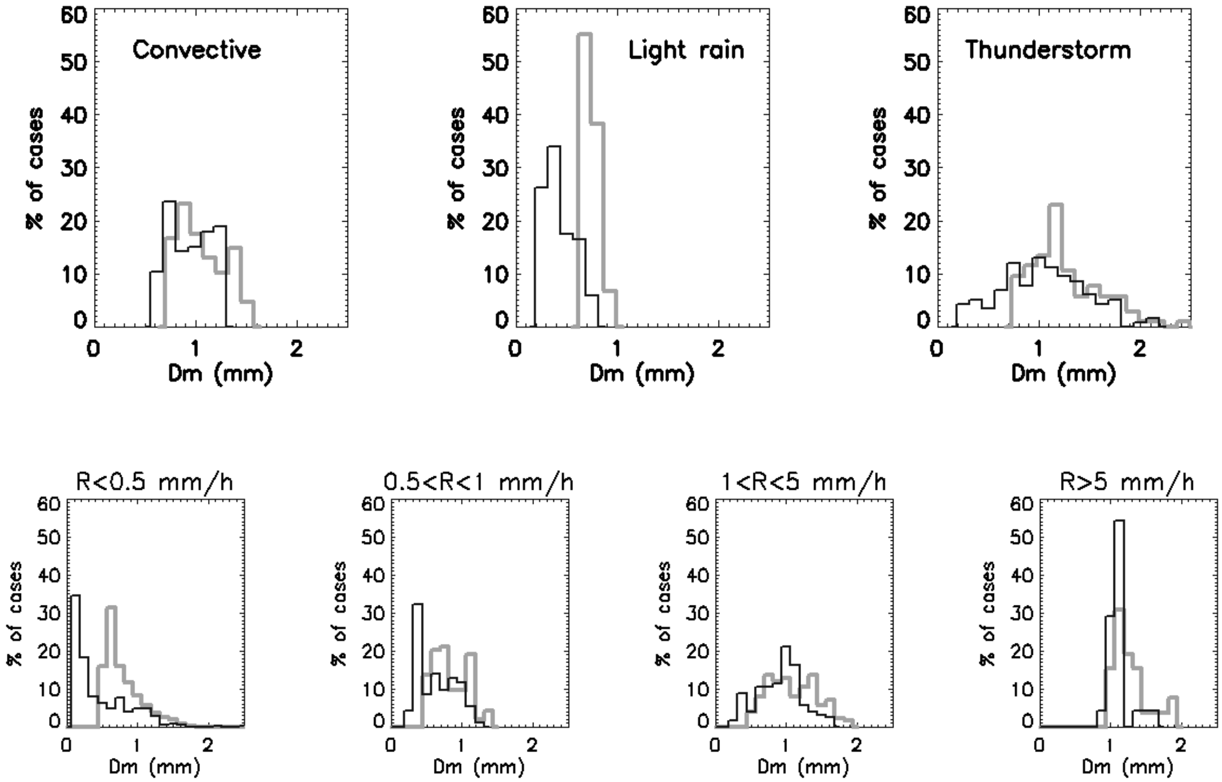


FIG. 7: $D_m$ histogram comparisons for three different rain types (as indicated in the top panels) and for different rainfall rate intervals (as indicated in bottom panels). The 2DVD data-based histograms are shown in grey and the combined MPS-2DVD DSD based histograms are shown in black. All histograms are based on 1-minute DSDs.

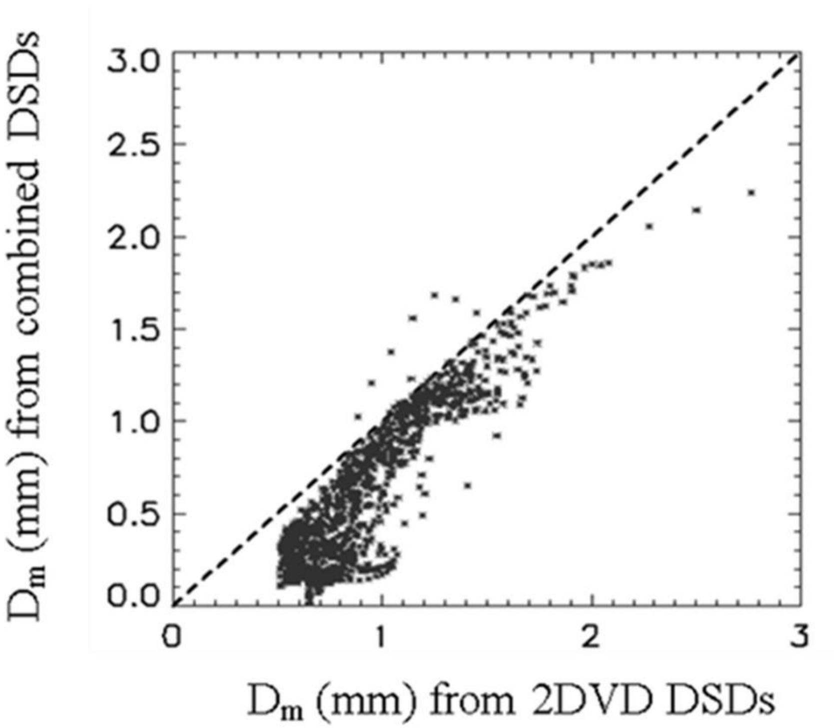


FIG. 8: $D_m$ comparisons between 2DVD-based and 2DVD-MPS combined DSD based estimates. Each data point is based on 1-min spectra.

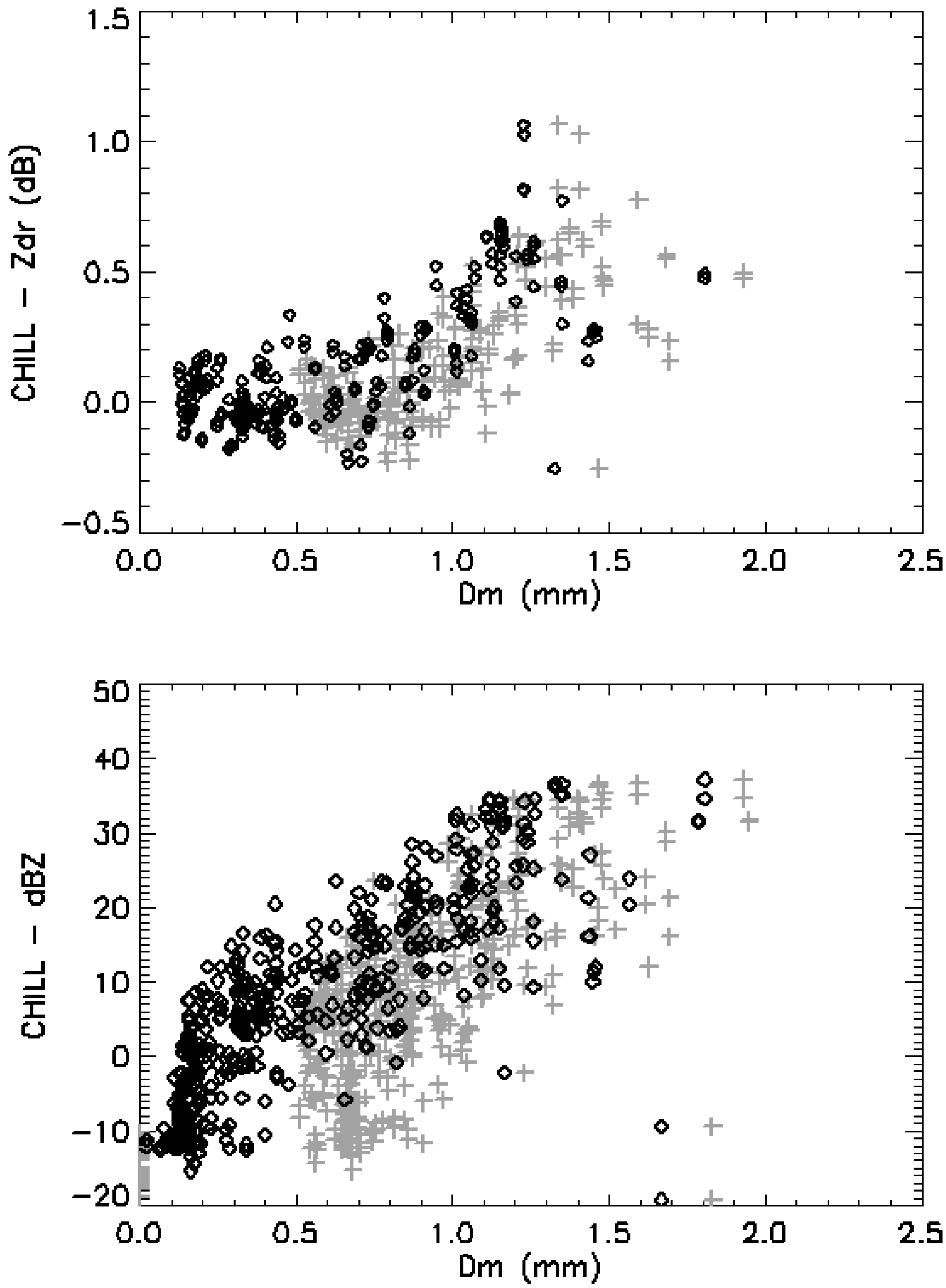


FIG. 9: (a) the CHILL S-band $Z_{dr}$ and (b) the CHILL S-band $Z_h$ measurements over the instrument site versus $D_m$ calculated using 2DVD (grey) and MPS-2DVD combined DSDs (black).

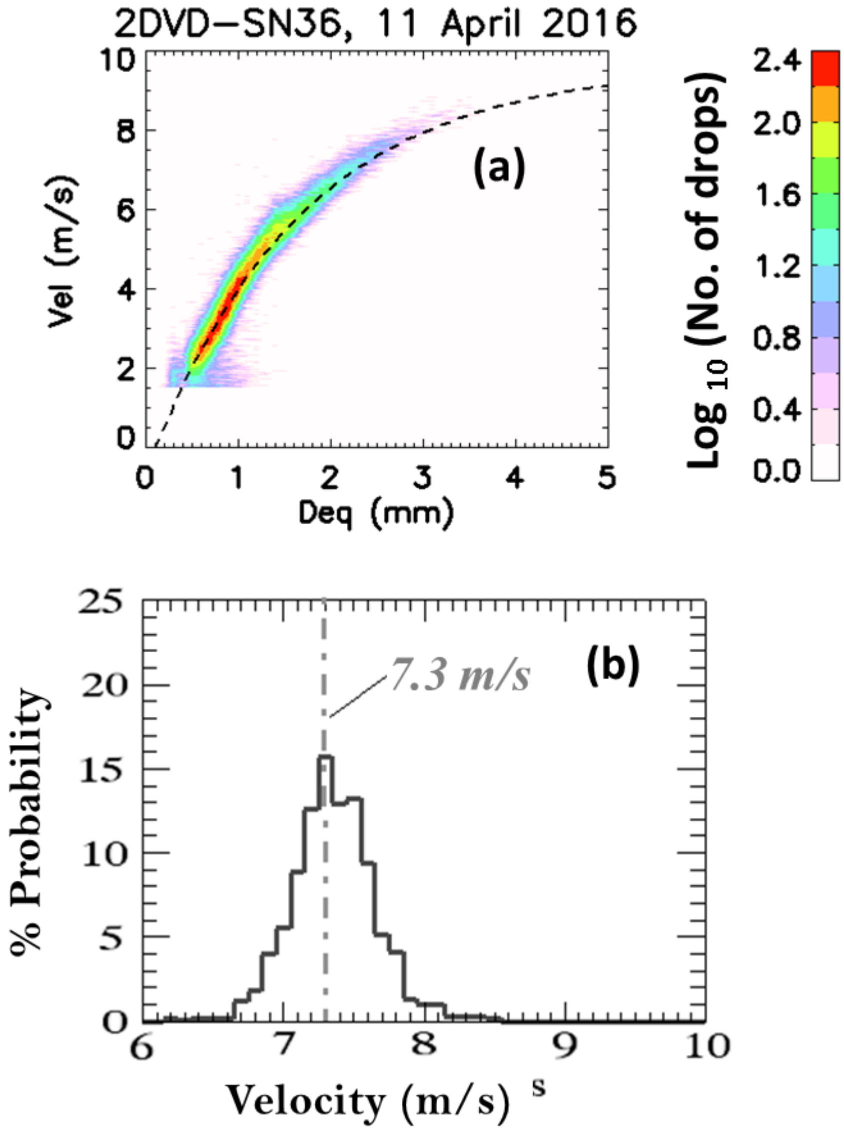


FIG. 10: (a) Fall velocity versus drop $D_{eq}$ from the 2DVD data as 2D frequency of occurrence plot. The dashed line represents the equation given in Atlas et al. (1973) which represents the Gunn-Kinzer variation, (b) histogram of vertical velocity specific to all drops with $D_{eq}$ values of 2.5 ± 0.1 mm. The expected value at sea level (7.3 m/s) is shown as dot-dash line.

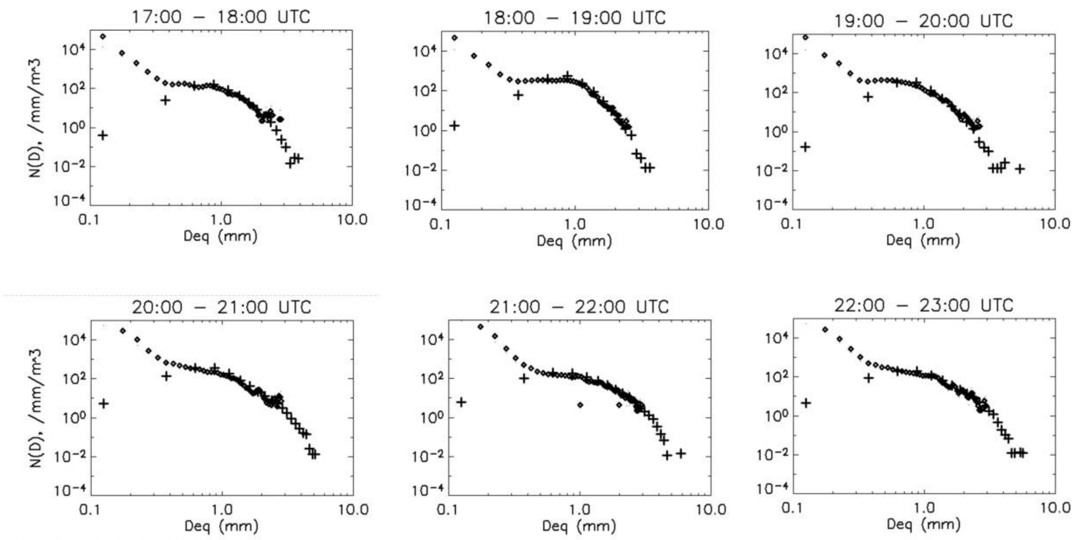


FIG. 11: Hourly DSD comparisons from the 2DVD (crosses) and 2DVD-MPS combined (diamonds) for the 11 April 2016 event in Huntsville. The time interval is specified for each case. The hourly rain accumulations were 1.3, 2.3, 1.6, 4.1, 4.4, and 3.7 mm for the 17, 18, 19, 20, 21, 22 hr UTC respectively.

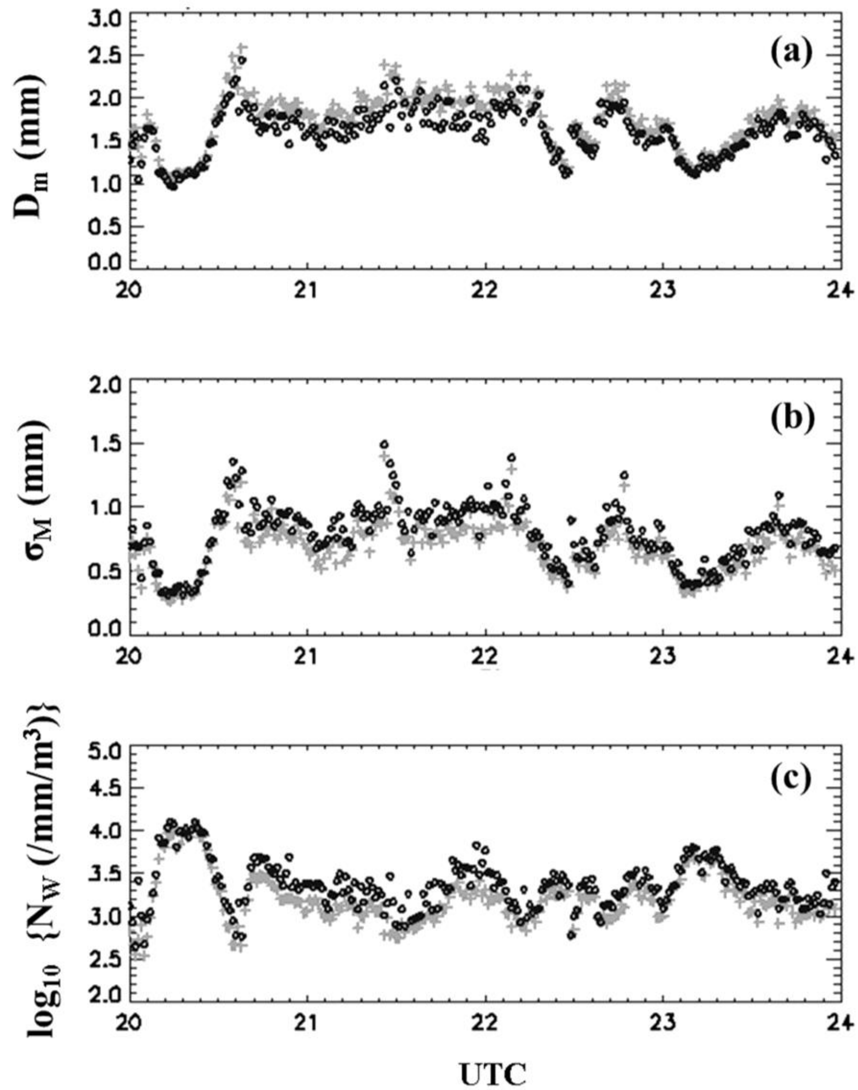


FIG. 12: (a) $D_m$ derived from 1 minute DSDs (after smoothing over 3 minutes) using 2DVD data alone (grey circles), and the combined MPS-2DVD data (black crosses); (b) the corresponding $\sigma_M$ values; (c) the corresponding $\log_{10}$ ($N_W$).

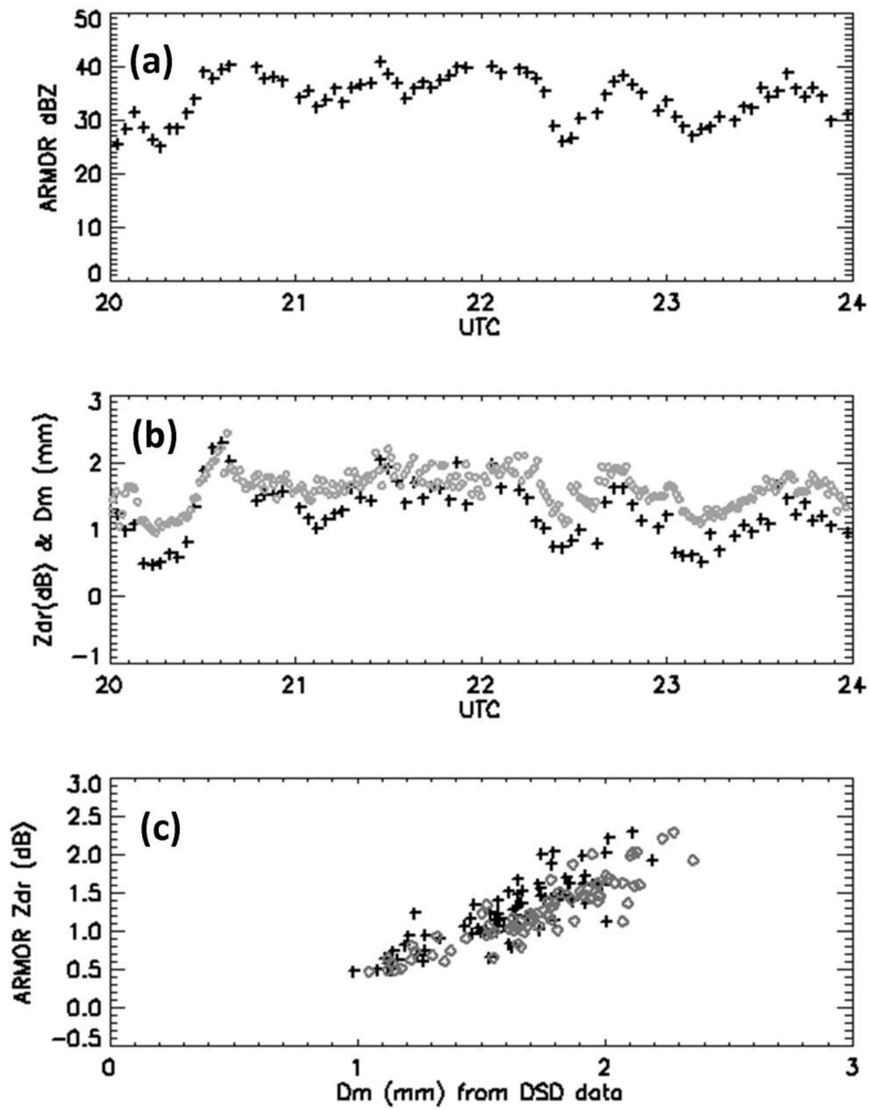


FIG. 13: (a) dBZ extracted over the MPS-2DVD site from the C-band ARMOR radar; (b) the corresponding $Z_{dr}$ (black crosses) and values of $D_m$ derived from the combined DSDs; (c) variation of the C-band $Z_{dr}$ with $D_m$ values from the 2DVD DSDs (grey) and the combined DSDs (black). Note that some of the scatter is due to radar measurement error.

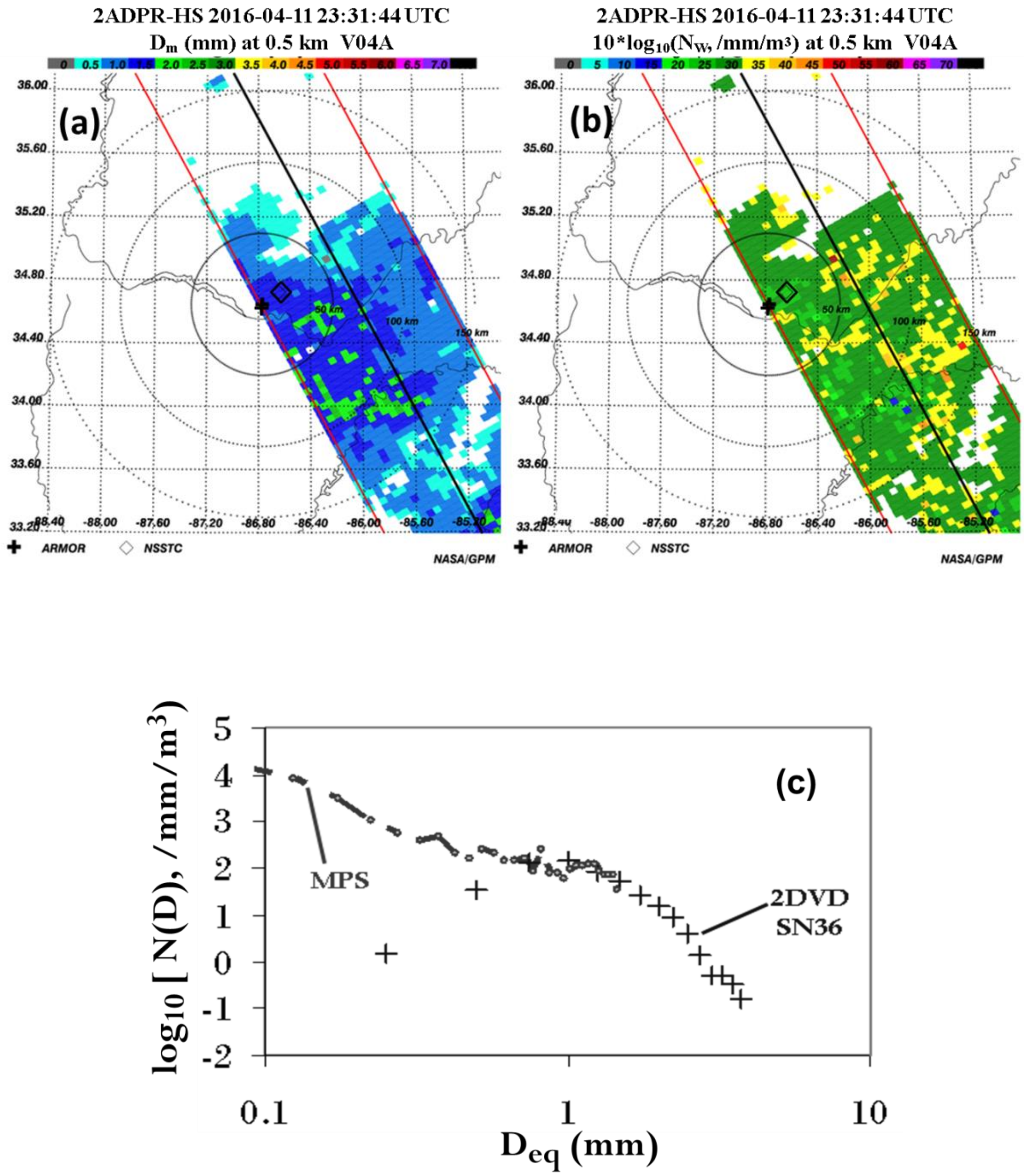


FIG. 14: The GPM DPR swath across northern Alabama during the 11 April, 2016 event showing a) $D_m$ [mm] and b) $10.\log_{10}(N_W)$ [$m^{-3}mm^{-1}$] both at 500-m AGL from the 2ADPR product, and (c) the 10-minute DSD from 23:25 – 23:35 UTC, from the MPS and 2DVD around the GPM overpass time period, at 23:31 UTC.

TABLE 1: Specifications of the MPS and 3rd generation low-profile 2DVD (SN36)

| **Parameter** | **MPS** | **2DVD (SN36)** |
|---|---|---|
| Number of active pixels | 62 | 625–630 |
| Clock/line scan frequency | Selectable, max 200 kHz (when matched to fall speed of 10 $ms^{-1}$) | 55.172 kHz |
| Horizontal resolution | 50 µm | 170 µm |
| Measuring area | 20 cm × 3.1 cm | 10 cm × 10 cm |
| Vertical resolution | 50 µm | Depends on fall speed (100 µm for 5 $ms^{-1}$) |
| Size range | 50 µm–3.1 mm | Typically > 0.6 mm |
| Calibration | Spinning glass disk with opaque dots of known size | Distance between vertical planes (i.e., plane test). Metal calibration spheres of known size |

TABLE 2: Dominant rain types during the two hour periods for the 17 April 2015 event, classified using CHILL RHI scans over the disdrometers.

| **2 hour period** | **Dominant Rain type** |
|---|---|
| 00 – 02 UTC | Dominated by melting snow<br>(not included in the DSD analyses) |
| 02 – 04 UTC | Moderately strong convective rain |
| 04 – 06 UTC | Moderately strong convective rain |
| 06 -08 UTC | Drizzle |
| 08 – 10 UTC | Light rain |
| 10 – 12 UTC | Fine drizzle |
| 12 – 14 UTC | Mostly stratiform rain |
| 14 – 16 UTC | Fine drizzle |
| 16 – 18 UTC | Mostly stratiform rain |
| 18 – 20 UTC | Thunderstorm |

TABLE 3: Two-hour rain accumulations for the three convective rain periods in Table 2

| **2-hr** | **SN36 (mm)** | **SN36 & MPS (m)** | **Pluvio (mm)** |
|---|---|---|---|
| 2-4 | 4.85 | 4.94 | 4.91 |
| 4-6 | 4.11 | 4.51 | 4.84 |
| 18-20 | 2.79 | 2.94 | 3.62 |